American Society of Hematology
2021 L Street NW, Suite 900,
Washington, DC 20036
Phone: 202-776-0544 | Fax 202-776-0545
editorial@hematology.org

Inhibition of p300/CREBBP catalytic activity drives context-dependent transcriptional activation in AML

Tracking no: BLD-2025-031924R2

Markus Meyerhöfer (University Medical Center Mainz, Germany) Yawen Zhou (University Medical Center of the Johannes Gutenberg University Mainz, Germany) Aaron Gallego-Crespo (Department of Hematology and Oncology, University Medical Center of the Johannes Gutenberg University Mainz, Germany) Viral Shah (University Medical Center Mainz, Germany) Malte Behrendt (University Medical Center of the Johannes Gutenberg University Mainz, Germany) Maria Saura-Pañella (University Medical Center of the Johannes Gutenberg University Mainz, Germany) Björn Häupl (Goethe University / DKFZ / DKTK, Germany) Oleksandr Todoriuk (University Medical Center Mainz, Germany) Monika Hartmann (University Medical Center Mainz, Germany) Matthias Klein (University Medical Center Mainz, Germany) Catherine Wölfel (University medical center JGU Mainz, Germany) Patricia Hähnel (University Medical Center Mainz, Germany) Christian Michel (University Medical Center Mainz, Germany) Sabine Muth (University Medical Center of the Johannes Gutenberg University Mainz, Germany) Thomas Kindler (University Medical Center of Mainz, Germany) Tobias Bopp (University Medical Center Mainz, Germany) Hansjörg Schild (Institute for Immunology, Germany) Sarah Horton (Cambridge Stem Cell Institute, United Kingdom) Markus Radsak (University Medical Center, Germany) Matthias Theobald (Johannes Gutenberg-University, Germany) George Vassiliou (University of Cambridge, United Kingdom) Brian Huntly (University of Cambridge, United Kingdom) Michael Kühn (Johannes Gutenberg-Universität Mainz, Germany) Falk Butter (Institute of Molecular Virology and Cell Biology, Friedrich-Loeffler-Institut,Greifswald, Germany) Thomas Oellerich (University Medical Center Frankfurt (Goethe University), Germany) Daniel Sasca (University Medical Center of the Johannes Gutenberg University Mainz, Germany)

Abstract:
The lysine acetyltransferase (KAT) activity of p300/CREBBP has traditionally been linked to transcriptional activation. This has been attributed largely to acetylation of histone residues such as H3K27ac, a defining hallmark of active regulatory elements. Here we show that, in acute myeloid leukemia (AML), inhibition of p300/CREBBP catalysis can paradoxically increase transcription. We combined time-resolved dynamics of nascent and total transcription with chromatin binding dynamics of p300/CREBBP and their associated TFs/co-regulators (inferred from chromatin pull-down proteomics, acetyl-proteomics and motif enrichment) to uncover mechanisms of transcriptional rewiring after p300/CREBBP catalytic inhibition. In parallel, we dissected the functional contribution of individual p300/CREBBP acetyl-interactome members to KAT inhibition using genome-wide CRISPR-Cas9 dropout and focused Perturb-seq screens. Together, these approaches revealed that KAT inhibition paradoxically retains p300/CREBBP and promotes cooperative TF assembly and increased H3K27 acetylation at a subset of regulatory elements. The effect was most pronounced at IRF motif-enriched loci, including interferon-stimulated genes (ISGs), where KAT inhibition triggered p300/CREBBP accumulation and enhanced combinatorial TF binding, enabling recruitment of the ISG activator STAT1. Consequently, ISG loci were converted into transcriptionally active states that induced cell-cycle arrest, differentiation and apoptosis. Therapeutically, combining KAT inhibition with interferon-alpha augmented ISG expression, synergistically drove AML cell death in vitro and significantly extended survival in both AML xenografts and murine models. These findings refine our understanding of p300/CREBBP KAT activity, demonstrating that cooperative TF assembly can reconfigure p300/CREBBP-containing complexes under catalytic inhibition to induce transcription, with translational implications for reprogramming interferon-driven programs through catalytic inhibition in AML and beyond.

Conflict of interest: COI declared - see note

COI notes: T. Oellerich received research funding from Gilead and Merck KGaA, is a consultant/received honoraria for/from Beigene, Roche, Janssen, Merck KGaA, Gilead, Kronos Bio and Abbvie (all not related to this work). D. Sasca reports personal honoraria from Abbvie, AstraZeneca, Blueprint, BMS, GSK, Gilead, Novartis and travel support from Abbvie, Novartis, AOP Pharma and Jazz Pharmaceuticals outside the submitted work. The remaining authors declare no potential conflicts of interest.

Preprint server: No;

Author contributions and disclosures: D.S. conceived the study, supervised the project and secured funding. M.M., Y.Z., A.G-C., V.S. and M.B. designed and performed experiments, with additional contributions from M.S-P., B.H., O.T., M.H., M.K., C.W., P.S.H. and F.B. M.M., A.G-C. and D.S. carried out bioinformatics analyses. C.M., S.M., T.K., T.B., H.J.S., S.J.H., M.R., M.T., G.S.V., B.J.P.H., M.W.M.K., F.B. and T.O. provided critical materials and/or intellectual input. D.S. wrote the initial manuscript draft. All authors reviewed and edited the final manuscript. M.M., Y.Z., A.G-C., V.S. and M.B. contributed equally to this work and share first authorship.

Non-author contributions and disclosures: No;

Agreement to Share Publication-Related Data and Data Sharing Statement: All raw and processed data files from genomics assays (RNA-Seq, SLAM-Seq, PRO-Seq and ChIP-Seq), CRISPR screens and Perturb-Seq experiments have been deposited in Gene Expression Omnibus (GEO) database under the accession GSE305384. Samples GSM5098267, GSM5098268 and GSM5098269 were previously deposited under accession GSE167163 and have been reused in this study. The custom open-source pipelines code used for data processing and downstream analysis has been deposited in a private GitHub repository and can be received upon request through email to the corresponding author.

Clinical trial registration information (if any):

Inhibition of p300/CREBBP catalytic activity drives context-dependent transcriptional activation in AML

M. Meyerhöfer[1,2*], Y. Zhou[1,2*], A. Gallego-Crespo[1,2*], V. Shah[1,2*], M. Behrendt[1,2*], M. Saura-Panella[1,2], B. Häupl[2,3,4,5], O. Todoriuk[1,2], M. Hartmann[1,2], M. Klein[6,7], C. Wölfel[1,2], PS. Haehnel[1,2], CS. Michel[1,2], S. Muth[6,7], T. Kindler[1,2,6], T. Bopp[2,6,7], H. Schild[6,7], SJ. Horton[8], M. Radsak[1,2,6], M. Theobald[1,2,6], GS. Vassiliou[8], BJP. Huntly[8], MWM. Kühn[1,2,6], F. Butter[9,10], T. Oellerich[2,3,4,5], D. Sasca[1,2,6,11]

1. Department of Hematology and Oncology, Medical Center of the Johannes Gutenberg University Mainz, Germany
2. German Cancer Consortium (DKTK), partner site Frankfurt/Mainz
3. Department of Medicine, Hematology and Oncology, University Hospital, Goethe University Frankfurt, Frankfurt am Main, Germany
4. Frankfurt Cancer Institute (FCI), Frankfurt am Main, Germany
5. German Cancer Research Center (DKFZ), Heidelberg, Germany
6. Research Center for Immunotherapy, Medical Center of the Johannes Gutenberg University Mainz, Germany
7. Institute of Immunology, Medical Center of the Johannes Gutenberg University Mainz, Germany
8. Department of Haematology and Cambridge Stem Cell Institute, University of Cambridge, Cambridge, UK
9. Institute of Molecular Biology, Mainz, Germany
10. Institute of Molecular Virology and Cell Biology, Friedrich-Loeffler-Institut, Greifswald, Germany
11. Institute for Quantitative and Computational Biosciences, Johannes Gutenberg University Mainz
* shared first authorship

Correspondence

Correspondence and requests for materials should be addressed to Daniel Sasca : dansasca@uni-mainz.de

Data sharing: All raw and processed data files from genomics assays (RNA-Seq, SLAM-Seq, PRO-Seq and ChIP-Seq), CRISPR screens and Perturb-Seq experiments have been deposited in Gene Expression Omnibus (GEO) database under the accession GSE305384. Samples GSM5098267, GSM5098268 and GSM5098269 were previously deposited under accession GSE167163 and have been reused in this study. The custom open-source pipelines code used for data processing and downstream analysis has been deposited in a private GitHub repository and can be received upon request through email to the corresponding author.

Keywords: p300/CREBBP; lysine acetyltransferase (KAT) inhibition; chromatin regulation; transcription factor assembly; interferon-stimulated genes (ISGs); AML

Key points

- Inhibition of p300/CREBBP catalysis causes their trapping at select regulatory elements, promoting cooperative transcription factor assembly
- At IRF motif-enriched loci, this facilitates H3K27 acetylation, STAT1 recruitment and activates interferon-stimulated gene transcription.

Abstract

The lysine acetyltransferase (KAT) activity of p300/CREBBP has traditionally been linked to transcriptional activation. This has been attributed largely to acetylation of histone residues such as H3K27ac, a defining hallmark of active regulatory elements. Here we show that, in acute myeloid leukemia (AML), inhibition of p300/CREBBP catalysis can paradoxically increase transcription. We combined time-resolved dynamics of nascent and total transcription with chromatin binding dynamics of p300/CREBBP and their associated TFs/co-regulators (inferred from chromatin pull-down proteomics, acetyl-proteomics and motif enrichment) to uncover mechanisms of transcriptional rewiring after p300/CREBBP catalytic inhibition. In parallel, we dissected the functional contribution of individual p300/CREBBP acetyl-interactome members to KAT inhibition using genome-wide CRISPR-Cas9 dropout and focused Perturb-seq screens. Together, these approaches revealed that KAT inhibition paradoxically retains p300/CREBBP and promotes cooperative TF assembly and increased H3K27 acetylation at a subset of regulatory elements. The effect was most pronounced at IRF motif-enriched loci, including interferon-stimulated genes (ISGs), where KAT inhibition triggered p300/CREBBP accumulation and enhanced combinatorial TF binding, enabling recruitment of the ISG activator STAT1. Consequently, ISG loci were converted into transcriptionally active states that induced cell-cycle arrest, differentiation and apoptosis. Therapeutically, combining KAT inhibition with interferon-alpha augmented ISG expression, synergistically drove AML cell death in vitro and significantly extended survival in both AML xenografts and murine models. These findings refine our understanding of p300/CREBBP KAT activity, demonstrating that cooperative TF assembly can reconfigure p300/CREBBP-containing complexes under catalytic inhibition to induce transcription, with translational implications for reprogramming interferon-driven programs through catalytic inhibition in AML and beyond.

Introduction

Acute myeloid leukemia (AML) is a proving ground for epigenetic therapy, where some of the greatest breakthroughs and also most striking setbacks have occurred[1-7].

Lysine acetyltransferases (KATs) are chromatin modifiers that facilitate transcriptional activation[8-12]. Among these, CREBBP and p300 have been central subjects of mechanistic studies for decades[9,13,14]. p300/CREBBP possess intrinsic lysine acetyltransferase activity and catalyze histone, TF and chromatin regulator acetylation[15-17]. This catalytic function typically drives dynamic transcriptional activation[16,17]. Besides their enzymatic role, they function as combinatorial signal integrators for TFs and chromatin

regulators through interaction domains[18-20]. In addition, their bromodomains (BRDs) recognize acetyl-lysine marks and stabilize p300/CREBBP on chromatin[21].

The development of clinical candidates targeting p300/CREBBP has been a long-standing priority; however, their large and complex protein structures posed substantial pharmacological challenges. Only recently have potent, selective KAT inhibitors been identified that block the acetyl-CoA binding site in a stereospecific manner[22,23]. In parallel, bromodomain inhibitors have become increasingly selective for p300/CREBBP[24,25]. Several BRD inhibitors are now in clinical testing (e.g. NCT06785636, NCT05488548, NCT03568656)[25,26], while first-generation KAT inhibitors are nearing the investigational-new-drug stage. However, clinical success in epigenetic therapy depends on three factors: clinically viable compounds, the right therapeutic context and excellent biological insight. When any of these elements is lacking, epigenetic drugs have often failed in trials[2,4,6]. Thus, a precise understanding of how p300/CREBBP regulate gene expression is more critical now than ever.

In transcriptional activation, pioneer TFs (e.g.,RUNX1/PU.1) bind their motifs even in nucleosome-occluded regions and initiate chromatin opening[27,28]. This enables recruitment of p300/CREBBP, which then help recruit additional TFs, integrate combinatorial TF signals, acetylate chromatin and promote transcription[29-31]. P300/CREBBP KAT activity, BRD „reader“ function and scaffolding domains contribute to this process[11,25,31,32]. However, while these domains are presumed to function in concert, conclusive evidence for coordinated activity is scarce. Moreover, although p300/CREBBP acetylate many substrates, their activity is most commonly associated with histone acetylation, particularly H3K27ac, a marker of active regulatory regions[33,34]. Still, mutating H3K27 to prevent its acetylation has no impact on gene expression, suggesting that histone acetylation may be more correlative than mechanistically essential, and that other, underappreciated events could be more functionally relevant[35].

Here, we follow a puzzling observation: in a subset of AMLs, catalytic p300/CREBBP inhibition triggers robust induction of interferon-stimulated genes (ISGs). This is counterintuitive, as p300/CREBBP are considered transcriptional coactivators, and their inhibition would be predicted to suppress, not activate, transcriptional programs. We therefore considered the possibility that, beyond their established roles in histone acetylation/activation p300/CREBBP catalytic activity may in certain contexts constrain transcription. Our data suggest that uncoupling catalytic acetylation from signal-integrating functions reveals unexpected biology and therapeutic opportunities, challenging long-held assumptions about p300/CREBBP in transcriptional regulation.

Methods

A complete list of antibodies, inhibitors, oligonucleotides, cells and software is provided in the Supplementary Key_Resources_Table.

Primary samples. Mononuclear cells from bone marrow or peripheral blood of AML/CMML patients were obtained with Ethics Committee approval (Rhineland-Palatinate, 2019_14110) and informed consent in accordance with the Declaration of Helsinki. Cells were cryopreserved in FBS/10% DMSO and cultured in StemSpan SFEMII+CD34$^+$ expansion supplements (UM729,SR1) and antibiotics.

In vivo studies. NSG (8-12 weeks) were bred in-house; C57BL/6J (8 weeks) were purchased. All procedures were approved by the National Investigation Office Rheinland-Pfalz (G24-1-015). NSG mice received 1×10^6 MOLM-13 cells i.v. after 2Gy irradiation. C57BL/6 received 0.5×10^6 Npm1c/Flt3-ITD leukemic cells after 5Gy. One week post-transplant, mice were randomized to vehicle, IFNa, KATi or combination for 15days. IFNa was given i.p. at 1×10^6U/kg every other day; KATi was given i.p. daily at 100mg/kg. Moribund animals were humanely euthanized. Survival was analyzed by Kaplan-Meier+log-rank testing.

Statistics and reproducibility. Unless indicated, n=3 independent biological replicates for cell-based assays. Two-group comparisons used unpaired two-tailed Student's t-tests; multiple groups used one-way ANOVA+Tukey's post-hoc test. RNA-seq/SLAM-seq were processed with DESeq2 with FDR control. CRISPR screen/Perturb-seq statistics are described in the Supplementary_Methods.

Data and code availability. Raw+processed data for RNA-seq, SLAM-seq, PRO-seq, ChIP-seq, genome-wide CRISPR screens and Perturb-seq have been deposited in GEO under accession GSE305384. Previously deposited samples (GSM5098267-GSM5098269;GSE167163) were re-used where indicated. Access details are provided in the Supplementary_Methods. Custom analysis code and pipelines are available upon request.

Comprehensive methods and step-by-step protocols are described in the Supplementary Methods.

Results

Inhibition of p300/CREBBP lysine acetyltransferase induces interferon-stimulated genes

In a recent study, we incidentally observed that KAT domain inhibition of p300/CREBBP with A-485 (hereafter KATi)[22] triggered a strong, unexpected ISG response within 24hr in a subset of AML models[31]. To rigorously confirm this paradoxical observation, we applied single-cell RNA sequencing (scRNA-seq) in two distinct AML cell lines: MOLM-13 (*KMT2A*-rearranged) and OCI-AML3 (*NPM1*-mutated). This confirmed a coordinated ISG upregulation across individual cells in response to KATi (Fig.1A-D,S1A). In parallel, we used quantitative mass spectrometry-based total proteomics in MOLM-13 to assess the corresponding protein-level changes. ISGs were robustly translated into protein, at the most significant changes from baseline (Fig.1E-F,S1B,Supp_Table_S11).

We next measured mRNA expression of *CXCL10*, a representative ISG, in 14 AML cell lines. KATi induced *CXCL10* in about half the models (Fig.1G), with a bias toward cell lines dependent on monocytic TFs such as IRF8, PU.1, MEF2D and CEBPA (Fig.1H,S1C). An independent KAT inhibitor, CPI-1612[36], produced similar induction of *CXCL10* in a dose-dependent manner (Fig.1I), confirming that the effect was compound class-specific. For all CPI-1612 experiments, the inactive (S,S)-CPI-1612 isomer was used as class-matched control.

Notably, p300 showed a preferential role in AML: among 1,136 cancer cell lines, p300 and MCM3AP were the only KAT enzymes whose genetic depletion impaired viability more in myeloid leukemia models (n = 42) than in other cancer types (Fig.S1D). p300 also ranked among the stronger depleting KATs overall.

To test whether ISGs contribute to the KATi response, we generated doxycycline-inducible, RNAi-based *STAT1* knockdown MOLM-13 and OCI-AML3 cell lines (Fig.1J,S1E-F). STAT1-deficient cells showed blunted *CXCL10* induction and significantly higher ATP signals compared to scrambled shRNA controls (Fig.1K-L).

ISG release is associated with p300/CREBBP catalytic inhibition in the presence of an intact scaffolding/signal-integrating platform

To determine whether ISG expression depends on the catalytic activity or signal-integrating functions of p300/CREBBP, we compared the effects of KATi with those of two orthogonal compounds: a bromodomain inhibitor in clinical testing (Inobrodib, hereafter BRDi)[25], which interferes with chromatin-based signal integration refined by KAT activity, and a PROTAC-based degrader of p300/CREBBP (Deg)[37], which disrupts catalytic+scaffolding functions (Fig.2A). For Deg, we confirmed p300 degradation kinetics by immunoblot (Fig.S2E). All three compounds reduced ATP across 8 AML cell lines; the only difference was that KATi had a broader therapeutic window (Fig.2B,S2A).

We then performed thiol(S)-linked alkylation for metabolic RNA sequencing (SLAM-Seq) at baseline and at 2, 12 and 24hr of treatment in MOLM-13. SLAM-Seq measures both nascent and total RNA, making it well suited to track the kinetics of ISG induction within 24hr. We performed gene set enrichment analyses for each time point relative to baseline. All three compounds reduced expression of canonical p300/CREBBP targets in AML. The most enriched gene sets involved MYC- and E2F-driven programs, inflammatory genes and G2/M regulators (Fig.2C,Supp_Table_S1-2). A distinct pattern emerged for transcriptional activation: KATi induced a strong and sustained increase in ISG transcription, whereas BRDi/Deg had minimal effects (Fig.2D-E,S2C-D,Supp_Table_S3-4). Kinetic analyses, based on a time-resolved average score of the top 26 ISGs or individual genes such as *IFIT3*, confirmed that KATi uniquely triggered a time-dependent increase in transcription (Fig.2E,S2B). Similarly, *CXCL10* expression remained unchanged across BRDi and Deg concentrations, as measured by qPCR (Fig.S2F). To test whether KATi-driven ISG induction also involved altered mRNA stability, we performed actinomycin D chase in MOLM-13. *CXCL10* decay was comparable between DMSO- and KATi-treated cells, whereas *IFIT3* decay was modestly faster with KATi, supporting increased transcriptional output as the primary ISG driver (Fig.S2G).

We also performed RNA-seq following BRDi or KATi versus DMSO in OCI-AML3 and MOLM-13. Again, both compounds downregulated MYC/E2F targets and G2/M checkpoints, but only KATi induced a distinct ISG boost. Heme metabolism and TNF signaling via NF-κB were enriched with both compounds (Fig.S2H-I), indirectly supporting the specificity of the ISG response to catalytic inhibition.

Moreover, at 24hr, we compared induction of *CXCL10*, *IFIT3* and *OAS3* in MOLM-13/OCI-AML3 with KATi versus 15 additional compounds, including agents with established differentiation-inducing activity in AML. KATi produced markedly stronger ISG induction than any comparator (Fig. S2J-K).

We next treated MOLM-13 cells with KATi in combination with either Deg or BRDi within the same 24hr period (Fig.2F). Compounds were either added simultaneously at hour 0 (co-treatment for 24hr), or

sequentially, with KATi first, followed by Deg/BRDi at 4/12/20hr. Strikingly, in all conditions where Deg was introduced, *CXCL10* expression was fully abrogated by the 24hr mark (Fig.2G). BRDi also significantly alleviated the KATi-induced release, albeit incompletely (Fig.2H). These results are critical: even a brief loss of p300/CREBBP protein, as short as 4hr at the end of the 24hr period, was sufficient to reverse the KATi-induced ISG expression.

KAT inhibition retains p300/CREBBP at IRF motif-enriched, immune regulatory elements

So far, we showed that ISG induction tracked with catalytically inactive but signal-integrating-competent p300/CREBBP. To understand how this occurs, we performed a comparative deconvolution of p300/CREBBP-associated chromatin processes following KATi. We initially defined a chromatin-regulatory network involving p300/CREBBP by integrating three data types: association proteomics, acetylproteomics and TF motif-inference at p300/CREBBP binding sites (Fig.3A).

We began with rapid immunoprecipitation mass spectrometry of endogenous proteins (RIME) after pulling down p300 in MOLM-13 and OCI-AML3 cells. We found consistent interactions with CREBBP, NONO and canonical BAF(cBAF) components such as SMARCA4/ARID1A (Fig.3B,S3A,Supp_Table_S5-6). The cBAF signal was in fact so dominant that it saturated the pulldown. To increase resolution, we repeated RIME in MOLM-13, this time targeting ARID1A. This revealed a broader set of indirect interactors, including IRF2BP1, IRF2BP2, IRF8, CEBPA and co-repressors TRIM33/TRIM28 (Fig.3C,Supp_Table_S7).

Next, we conducted SILAC-based acetylproteomics in DMSO- or KATi-treated MOLM-13 and OCI-AML3. p300 and CREBBP were among the most significantly acetylated proteins, showing reduced (auto)acetylation upon KATi (Fig.3D,Supp_Table_S9-10). Other highly significant acetylation targets were RUNX1, MEF2D, TRIM33, TRIM28, NONO, KMT2C, IRF2BP2, ARID1A and SMARCA4 (Fig.3D,Supp_Table_S9-10).

We then performed ChIP-seq for p300 and CREBBP in MOLM-13 and OCI-AML3 treated with DMSO or KATi. CREBBP exhibited more binding sites and the majority of p300 sites were co-bound by CREBBP (Fig.S3B). The motif enrichment patterns were highly similar between the two, with one exception: CREBBP showed strong enrichment for CTCF motifs, while p300 did not. Aside from this difference, ETS and CEBP motifs ranked highest, followed by bZIP, RUNX and IRF motifs, while MEF, MYB and HOX motifs ranked lower but remained highly significant (Fig.3E,Supp_Table_S12-13). Motif profiles at shared ("common") peaks closely resembled those of p300 alone (Fig.3F). Based on their consistent motif enrichment, we included PU.1+FLI1 (for ETS motif) and CEBPA+CEBPB (CEBP motif), in the proposed p300/CREBBP-associated chromatin network.

Finally, by integrating acetylproteomics, RIME and ChIP-seq/motif-enrichment data, we constructed a p300/CREBBP "acetyl-interactome" of 17 TFs+co-regulators: p300, CREBBP, ARID1A, SMARCA4, IRF2BP2, IRF2BP1, IRF8, MEF2D, PU.1, FLI1, RUNX1, CEBPA, CEBPB, TRIM28, TRIM33, NONO and KMT2C (Fig.3G).

We also assessed chromatin binding dynamics at p300-, CREBBP- and common peaks. Strikingly, following KATi, p300/CREBBP had increased binding at many loci in both cell lines (Fig.3H,S3C-D). Among

the top 10% most retained sites, the majority were mapped to distal regulatory elements and ~15% at promoters (Fig.3I). These regions were highly enriched for immune-related ontologies; all top 20 overrepresentation terms involved immune, defense or inflammatory processes (Fig.3J,S3E). At key loci (a common CXCL enhancer, *IRF2BP2* promoter and lncRNA *LNCATV* in OCI-AML3, *IFIT3* promoter in MOLM-13), we confirmed increased p300/CREBBP binding after KATi by ChIP-qPCR (Fig.S3F-G).

Finally, we analyzed TF motif enrichment at the top 10% most retained p300-, CREBBP- and common-binding sites. While the same motifs as in the full catalogues were again detectable, the enrichment landscape shifted. Nearly all motifs lost prominence except for IRF, which consistently increased across all scenarios (Fig.3K,Supp_Table_S14-15).

Inhibition of p300/CREBBP catalytic activity promotes combinatorial TF assembly and transcription at IRF motif-marked regulatory sites

We wondered whether KATi-induced retention of p300/CREBBP on chromatin is associated with ISG induction. To map nascent transcription at promoters and enhancers and align it with p300/CREBBP dynamics, we performed PRO-Seq in MOLM-13 cells treated with DMSO or KATi. ISG regulatory elements were again among the most upregulated after KATi (Fig.4A). We then examined chromatin-binding dynamics of p300/CREBBP and nine additional members (RUNX1, PU.1, FLI1, IRF2BP2, ARID1A, IRF8, MEF2D, CEBPA, CEBPB), together with the histone modifications H3K27ac and H3K27me3, by ChIP-seq under DMSOvsKATi. H3K27ac is a canonical p300/CREBBP acetylation mark, whereas H3K27me3 represents a repressive mark on the same residue. For each factor, we calculated binding scores at differentially transcribed regions and quantified occupancy changes. At regions with decreased PRO-Seq signal, most factors showed reduced binding, consistent with transcriptional disengagement (Fig.4B). H3K27me3 remained unchanged, while H3K27ac showed the strongest reductions across all assayed signals (Fig.4B). In contrast, regions with increased transcription showed marked gains in factor occupancy. H3K27me3 remained unchanged, while H3K27ac increased substantially (Fig.4B). The TF occupancy dynamics were reproducible in OCI-AML3, even when using MOLM-13-derived PRO-Seq regions (Fig.4C).

We then performed motif enrichment of differentially transcribed regions. Regions with decreased transcription were enriched for MYB, ETS and MEF motifs, consistent with oncogenic programs dependent on p300/CREBBP acetylation (Fig.4D,Supp_Table_S16). Regions with increased transcription were enriched for ETS, KLF and IRF motifs (Fig.4F,Supp_Table_S17). We assessed binding dynamics of p300/CREBBP and acetyl-interactome members, and H3K27ac abundance, at these motif-defined regions. At loci where transcription decreased (MEF, MYB, ETSdown), we observed loss of TF/co-regulator binding and marked decrease of H3K27ac (Fig.4E,S4A). Conversely, at loci with increased transcription, TF/co-regulator binding was maintained or even enhanced, and H3K27 acetylation increased (Fig.4G,S4B). These patterns were most pronounced at IRF motif-enriched sites, which overlapped most closely with ISG regulatory elements (Fig.S4C). Here, KATi induced a strong retention of p300/CREBBP (~60% each), accompanied by gain in H3K27ac (~80%), while changes at ETS_up and KLF

motif regions were more modest (Fig.4G). Also, ARID1A and several TFs became stably retained on chromatin (Fig.4G). IRF2BP2 was the only factor whose occupancy was reduced at these sites (Fig.4G).

This pattern was evident at exemplar ISGs, including *OAS2, IFIT2/IFIT3* in MOLM-13 and the *IFIT1-5* cluster in OCI-AML3. Here, multiple regulatory elements showed increased occupancy of p300, CREBBP and several acetyl-interactome members, correlated with increased H3K27ac and transcriptional upregulation (Fig.4H,S4D). In contrast, canonical p300/CREBBP-dependent loci, such as *CST7, HES1, ADGRG3*, showed reduced factor occupancy, decreased H3K27ac and reduced transcription (Fig.4H).

We were intrigued by the paradoxical H3K27ac gain at IRF/ISG. Building on the 24hr KATivsDMSO conditions, we assessed H3K27ac after adding Deg for the final 4hr of each treatment (i.e., 24hr KATi/DMSO with Deg during the last 4hr), matching the ISG reversibility timing shown in Fig.2F-H. In ChIP-seq and ChIP-qPCR (+matched CREBBP ChIP-qPCR), late Deg addition returned the KATi-associated H3K27ac gain to baseline (Fig.4H-I). We then tested motif-marked differential PRO-seq regions. At MEF-associated downregulated regions, H3K27ac decreased across perturbations. In contrast, IRF-motif upregulated regions gained H3K27ac only under KATi, and this gain returned to baseline upon late Deg addition (Fig.4J).

Collectively, KATi reduces TF/co-regulator binding, H3K27ac and transcription at canonical targets but promotes complex assembly, H3K27ac accumulation and transcription at IRF/ISG regulatory elements. These gains implicate increased p300/CREBBP chromatin association and protein integrity.

Functional deconvolution of the p300/CREBBP acetyl-Interactome links ISG induction to combinatorial TF integrity

To dissect the functional contribution of individual members of the p300/CREBBP acetyl-interactome to KATi-induced ISG expression and AML cytotoxicity, we performed two complementary functional genomics screens: (i) a genome-wide CRISPR-Cas9 dropout screen±KATi, and (ii) a focused Perturb-seq screen targeting acetyl-interactome components with scRNA-seq readout (Fig.5A). For the dropout screen, MOLM-13 and OCI-AML3 were transduced with the Brunello sgRNA library and exposed to DMSOvsKATi. Under KATi, sgRNAs targeting PU.1 (*SPI1*) and *ARID1A* were significantly enriched in MOLM-13; *SMARCA4, MEF2D, p300* and *RUNX1* showed non-significant enrichment (Fig.5B, Supp_Table_S18). In OCI-AML3, *MEF2D* (significant), *ARID1A, SMARCA4*, PU.1, *RUNX1, p300* and *IRF8* (non-significant) showed similar enrichment patterns (Fig.S5A,Supp_Table_S20). This indicated that a broader subset of the acetyl-interactome contributed to mediating the KATi effects on viability. In contrast, sgRNAs targeting *IRF2BP2* (significant in both cell lines) and *CEBPA* (significant in MOLM-13, with a consistent trend in OCI-AML3) were depleted, suggesting that these factors counteracted the cytotoxic effects of KATi (Fig.5B,S5A,Supp_Table_S18,20).

To test specificity, we repeated the dropout screen with BRDivsDMSO. The enrichment pattern changed markedly: *IRF2BP2* was most enriched, followed by *IRF2BP1* and *CEBPA*. In contrast, *SPI1*, *ARID1A*, *SMARCA4*, *IRF8* and *MEF2D* were unaffected and *p300* and *RUNX1* were significantly depleted, followed by *FLI1* and *CREBBP* (Fig.5C,Supp_Table_S19).

Perturb-seq was performed in MOLM-13 cells, targeting all 17 acetyl-interactome components plus non-targeting controls. ScRNA-seq was conducted under DMSO and KATi. The composite "ISG score" defined in Fig.1A (top 26 ISGs upregulated by KATi) was used for comparison. No changes in ISG expression were seen in the DMSO condition.

Under KATi, knockout of *ARID1A*, *SMARCA4*, PU.1, *IRF8* (and partly *RUNX1/MEF2C*) blunted ISG induction, while knockout of *CEBPA* and *IRF2BP2* amplified it (Fig.5D,S5B). *ARID1A* knockout also mitigated KATi-induced downregulation of canonical programs, e.g. MYC/E2F targets and G2/M checkpoints (Fig.S5B).

As cBAF components (ARID1A/SMARCA4) repeatedly emerged in the mechanism of response to KATi, we tested whether cBAF deficiency impairs KATi response. We co-treated MOLM-13 and OCI-AML3 with KATi and a chemical degrader of BRG1 (degBRG1) and assessed interaction. In both cell lines, BRG1 degradation attenuated the KATi-associated ATP signal decrease (Fig.5E).

To explore how BAF components acquired ISG-regulatory capacity upon KATi (Fig.5F), we performed RIME for ARID1A in MOLM-13 treated with DMSOvsKATi. KATi induced new chromatin-proximal interactions between ARID1A and ISG effectors such as ISG15, IFI16, MX2 and STAT1 (Fig.5G,Supp_Table_S8). We validated STAT1 involvement by western blot: total STAT1 levels increased dose-dependently after 24hr KATi, consistent with its identity as an ISG, while phospho-STAT1 levels also rose, indicating activation (Fig.5H,S5C).

Moreover, we detected de novo STAT1 binding via ChIPSeq at IRF motif-marked regions corresponding to loci with significantly increased transcription in our PRO-seq data (Fig.5H). This was highly specific to IRF motif-containing loci, as compared to both motif-defined downregulated regions and other upregulated regions lacking IRF motifs. For instance, STAT1 showed strong de novo occupancy at the promoters of *OAS2*, *IFIT3* and *STAT1* itself, consistent with a feed-forward loop of transcriptional activation triggered by catalytic inhibition of p300/CREBBP (Fig.5J).

Finally, we addressed directionality with dependency experiments. p300/CREBBP degradation during the final 4hr of 24hr KATi exposure collapsed STAT1 ChIP-qPCR occupancy at *IFIT3/OAS2* to baseline; meanwhile, STAT1 knockdown did not reduce CREBBP occupancy at the same loci under KATi (Fig.5K-L).

In conclusion, KATi promotes combinatorial TF/co-regulator activity at IRF motif-marked regions (including ISGs), enables de novo recruitment of pro-ISG transcriptional modulators such as STAT1 and sustains transcriptional activation.

Exogenous Interferon-alpha enhances KATi-Induced ISG activation and apoptosis

We tested the effects of KATi on apoptosis, cell cycle and differentiation. Two 'physiological' concentrations (250nM and 500nM), which reduced viability by ~IC65-IC90 (Fig.S2A), were compared with a higher dose (1000nM) that triggered the strongest ISG response. At 24hr (the mechanistic time point) G1 arrest was minimal, ATP signal was unchanged (OCI-AML3) or modestly reduced (MOLM-13) and apoptosis and CD11b/CD14 remained at baseline (Fig.6A,S6A-D). Starting with 48hr, apoptotic and cell cycle effects became prominent at 1000nM, while lower doses had minimal impact (Fig.6A,S6A-B).

As of 72hr, all doses promoted signs of differentiation by Giemsa staining and CD14/CD11b expression, though effects were more pronounced at 1000nM (Fig.6B-C,S6E-F). This prompted us to ask whether the ISG response (and possibly treatment efficacy) could be enhanced at lower KATi concentrations. With KATi releasing ISG expression, we reasoned that exogenous interferon-alpha (IFNa) could further boost this response (Fig.6D). We treated MOLM-13 and OCI-AML3 cells with IFNa in combination with 500nM KATi. Strikingly, the combination induced logarithmic upregulation of *CXCL10* and significantly enhanced apoptosis in both cell lines (Fig.6E-F,S6G). We tested the same strategy using CPI-1612 with IFNa. In both qPCR (*CXCL10*) and Annexin V/7-AAD assays, CPI-1612+IFNa combination mirrored the results of KATi+IFNa, with massive ISG upregulation and a dramatic increase in apoptotic fractions (Fig.6E-F,S6G).

We then expanded these combinations to 6 additional AML cell lines, 3 with high and 3 with low baseline ISG responsiveness. The combination of either KATi or CPI-1612 with IFNa induced logarithmic *CXCL10* upregulation and significantly enhanced apoptosis in all high and one low ISG cell lines (Fig.6G-I). Finally, we evaluated synergy using a combination matrix of KATi/CPI-1612 with IFNa in MOLM-13 and OCI-AML3 cells. In both models, the combinations yielded high synergy scores (Fig.6J).

KAT inhibition combined with interferon-alpha demonstrates efficacy in-vivo and ex-vivo

We also assessed the in-vivo efficacy of the KATi+IFNa combination in NSG mice transplanted with MOLM-13. Single-agent KATi/IFNa produced only modest responses, while their combination markedly prolonged survival (Fig.7A). Even at death, mice in the combination group showed reduced leukemic infiltration in spleen and peripheral blood, while bone marrow involvement was similar across groups (Fig.7B,S7A). We next tested KATi+IFNa in a genetically defined murine AML model driven by *Npm1c+Flt3*-ITD[38,39]. In vitro, KATi+IFNa cooperatively increased *CXCL10* expression (Fig.7C). Combination matrices using either KATi or CPI-1612 with IFNa showed synergistic suppression of AML viability (Fig.7D,S7B).

Also in-vivo, KATi+IFNa significantly prolonged survival compared to control and IFNa-treated mice, while single KATi did not (Fig.7E).

We extended these findings to 7 primary AML and 4 CMML samples. KATi+IFNa significantly increased ISG expression, reduced ATP signals and induced apoptosis (Fig.7F-K,S7C-E). CD11B responses were variable, increased in general with KATi alone and did not consistently increase further with the combination (Fig.S7F). Across three CMML samples, the combination nearly abolished colony numbers and cellularity in colony formation assays, outperforming either monotherapy (Fig.7L,S7G). Altogether, these results uncover an unexpected therapeutic strategy: combining p300/CREBBP KAT inhibition with IFNa induced a potent ISG response and enhanced apoptosis.

Discussion

For decades, the p300/CREBBP catalytic activity has been considered mainly in terms of histone acetylation, and this view has shaped much of the field. Yet the true contribution of the p300/CREBBP catalysis to transcriptional regulation has not been sufficiently resolved. Using matched inhibitors and a reference degrader, we assessed domain-specific functions of p300/CREBBP in AML. Catalytic inhibition

revealed a non-canonical role of the KAT domain: it paradoxically increased TF and co-regulator assembly at specific loci and boosted transcription. Thus, in certain contexts, inhibition of p300/CREBBP KAT activity leads to transcriptional activation.

These insights have potential translational relevance. Combining p300/CREBBP KAT inhibition with IFNa synergistically enhances ISG expression, induces apoptosis and reduces leukemic burden, supporting further evaluation. In clinical practice, IFNa is a standard treatment for polycythaemia vera and essential thrombocythemia[40-43]. It also shows efficacy and is occasionally used in chronic myeloid leukemia, for example during pregnancies[44]. Although IFNa has shown limited benefit in other myeloid neoplasia[45-47], our findings indicate that KAT inhibition creates a therapeutic context in which IFN biology becomes therapeutically actionable. Moreover, targeting p300/CREBBP catalysis versus scaffolding may be valuable in diseases where interferon responses are beneficial (e.g. autoimmune/infectious).

Mechanistically, prior studies indicated that H3K27ac is not universally required for gene expression[35]. In addition, p300/CREBBP can exert inhibitory effects through catalysis-independent mechanisms, e.g. Polycomb-type repression[48]. We therefore initially considered whether these models might explain the transcriptional changes observed after KATi. We observed no change in H3K27me3 and, surprisingly, increased H3K27ac at IRF-associated regions. At first glance, this might appear to reaffirm a familiar principle -that H3K27ac tracks with active transcription- but one nuance is central: p300/CREBBP chromatin binding, H3K27ac and transcription all increase under enzymatic inhibition that would be expected to repress them, and this state appears contingent on p300/CREBBP integrity. To our knowledge, this is the first demonstration of such biology under p300/CREBBP KAT inhibition.

More broadly, we observed increased p300/CREBBP retention following KATi, even at loci without transcriptional activation. We use ‘retention‘ operationally to denote increased ChIP-based occupancy, without inferring residence-time kinetics or excluding redistribution. This phenotype has also been noticed by others[17] and is consistent with a recent elegant single-molecule tracking study showing that p300/CREBBP catalytic activity counteracts chromatin binding[49]. This suggests an analogy to PARP1 ‘trapping’ by class I PARP inhibitors, where enzymatic inhibition prevents release from DNA[50]. PARP trapping varies between compounds, and analogous compound-specific differences may apply to KAT inhibitors, with implications for treatment efficacy and toxicity.

KAT inhibition boosts ISG transcription. This is paradoxical: p300/CREBBP are established co-activators for STAT-driven transcription, and one would predict that loss of their catalytic activity should dampen ISG expression[51-53]. We propose that the signal-integrating functions of p300/CREBBP sustain ISG activation, whereas their catalytic activity limits STAT1 binding to chromatin. This mechanism may reflect a physiological requirement to terminate feed-forward ISG release once the interferon response has been initiated. Meanwhile, IRF2BP2 apparently counteracts the effects of KATi. Loss of IRF2BP2 amplified ISG expression and increased sensitivity to KATi, while its depletion from ISG loci after KATi contrasted with the increased occupancy of most other acetyl-interactome members, underscoring its repressive function. This positions IRF2BP2 as a critical checkpoint that balances ISG regulation in AML and supports the work of Ellegast et al., who identified IRF2BP2 as a key suppressor of intrinsic inflammation in AML[54].

Our time-resolved SLAM-seq data show distinct kinetics: canonical p300/CREBBP-dependent programs respond rapidly, whereas the IRF/ISG module becomes evident only after ~12hr. We interpret this delay as consistent with a multi-step process in which sustained catalytic inhibition progressively establishes a permissive IRF/ISG regulatory state. At the same time, we acknowledge a plausible alternative interpretation: the IRF/ISG response may reflect an early differentiation-associated transcriptional shift, consistent with IRF-linked myelomonocytic programs that can precede overt surface-marker changes. We therefore frame the acute IRF/ISG program as an inhibited-state response that emerges within the first 24hr of treatment, while recognizing that early state changes may contribute to the kinetics and lineage bias.

Several important questions remain unresolved. Despite functional overlap, p300 and CREBBP have partly distinct roles[55-57]; selective PROTACs targeting each protein individually may help disentangle their contributions - something current KAT inhibitors cannot achieve. A biological question is whether, in line with the established "hit-and-run" mechanism of acetylation[15], p300/CREBBP-mediated acetylation promotes their release from bound sites - an activity we may have previously misinterpreted. Why does H3K27ac increase at IRF-associated hubs under KATi? Is this due to a hub-specific conformation that preserves p300/CREBBP acetyltransferase function, exclusion of HDAC or compensatory acetylation by other KATs? Furthermore, do other KAT enzymes become similarly "retained" when their catalytic domains are blocked? Addressing these questions could uncover new therapeutic opportunities across cancers.

Overall, we show that enzymatic inhibition of p300/CREBBP can paradoxically activate transcription by shifting the TF-cofactor balance toward a pro-transcriptional state. At ISGs, KATi reinforces p300/CREBBP retention alongside key TFs/co-regulators, facilitating H3K27ac and recruitment of ISG-promoting factors such as STAT1. This stable chromatin engagement sustains a feed-forward loop of ISG expression. Finally, our findings provide mechanistic and therapeutic rationale for combining KAT inhibition with IFNa.

Acknowledgements

This work was supported by a grant of the German Research Foundation (DFG 510093527, Emmy Noether Program) and a sponsorship of the Foundation Future without Cancer Mainz (WVHF_05_2023) to D. Sasca. S. Muth, T. Bopp, H. Schild, M. Radsak, M. Theobald, MWM. Kühn and D. Sasca are investigators of the CRC 1292 of the German Research Foundation (DFG 318346496).

The authors thank the sequencing core facility of the University Medical Center Mainz, and Pamela Aranda-Lopez from the flow cytometry laboratory of the Department of Hematology and Oncology, University Medical Center Mainz, for their support. They also thank Martine Pape and Marion Bodach from the DKTK Proteomics Platform Frankfurt and Uwe Plessmann from the Bioanalytical Mass Spectrometry Group, MPI-NAT Göttingen (Prof. Henning Urlaub), for technical assistance with sample preparation and LC/MS measurements.

AI-assisted tools (ChatGPT, OpenAI v4/v5) were used for grammar/language polishing and code debugging; all outputs were reviewed and verified by the authors.

Author contributions

D.S. conceived the study, supervised the project and secured funding. M.M., Y.Z., A.G-C., V.S. and M.B. designed and performed experiments, with additional contributions from M.S-P., B.H., O.T., M.H., M.K., C.W., P.S.H. and F.B. M.M., A.G-C. and D.S. carried out bioinformatics analyses. C.M., S.M., T.K., T.B., H.S., S.J.H., M.R., M.T., G.S.V., B.J.P.H., M.W.M.K., F.B. and T.O. provided critical materials and/or intellectual input. D.S. wrote the initial manuscript draft. All authors reviewed and edited the final manuscript.

M.M., Y.Z., A.G-C., V.S. and M.B. contributed equally to this work and share first authorship.

Conflict of interest disclosure

T. Oellerich received research funding from Gilead and Merck KGaA, is a consultant/received honoraria for/from Beigene, Roche, Janssen, Merck KGaA, Gilead, Kronos Bio and Abbvie (all not related to this work).

D. Sasca reports personal honoraria from Abbvie, AstraZeneca, Blueprint, BMS, GSK, Gilead, Novartis and travel support from Abbvie, Novartis, AOP Pharma and Jazz Pharmaceuticals outside the submitted work. The remaining authors declare no potential conflicts of interest.

References

1. Dombret H, Seymour JF, Butrym A, et al. International phase 3 study of azacitidine vs conventional care regimens in older patients with newly diagnosed AML with >30% blasts. *Blood*. 2015;126(3):291-299.
2. Stein EM, Garcia-Manero G, Rizzieri DA, et al. The DOT1L inhibitor pinometostat reduces H3K79 methylation and has modest clinical activity in adult acute leukemia. *Blood*. 2018;131(24):2661-2669.
3. DiNardo CD, Jonas BA, Pullarkat V, et al. Azacitidine and Venetoclax in Previously Untreated Acute Myeloid Leukemia. *N Engl J Med*. 2020;383(7):617-629.
4. Salamero O, Molero A, Perez-Simon JA, et al. Iadademstat in combination with azacitidine in patients with newly diagnosed acute myeloid leukaemia (ALICE): an open-label, phase 2a dose-finding study. *Lancet Haematol*. 2024;11(7):e487-e498.
5. Montesinos P, Recher C, Vives S, et al. Ivosidenib and Azacitidine in IDH1-Mutated Acute Myeloid Leukemia. *N Engl J Med*. 2022;386(16):1519-1531.
6. Dawson MA, Borthakur G, Huntly BJP, et al. A Phase I/II Open-Label Study of Molibresib for the Treatment of Relapsed/Refractory Hematologic Malignancies. *Clin Cancer Res*. 2023;29(4):711-722.

7. Issa GC, Aldoss I, DiPersio J, et al. The menin inhibitor revumenib in KMT2A-rearranged or NPM1-mutant leukaemia. *Nature*. 2023;615(7954):920-924.
8. Brownell JE, Zhou J, Ranalli T, et al. Tetrahymena histone acetyltransferase A: a homolog to yeast Gcn5p linking histone acetylation to gene activation. *Cell*. 1996;84(6):843-851.
9. Ogryzko VV, Schiltz RL, Russanova V, Howard BH, Nakatani Y. The transcriptional coactivators p300 and CBP are histone acetyltransferases. *Cell*. 1996;87(5):953-959.
10. Visel A, Blow MJ, Li Z, et al. ChIP-seq accurately predicts tissue-specific activity of enhancers. *Nature*. 2009;457(7231):854-858.
11. Wang L, Gural A, Sun XJ, et al. The leukemogenicity of AML1-ETO is dependent on site-specific lysine acetylation. *Science*. 2011;333(6043):765-769.
12. MacPherson L, Anokye J, Yeung MM, et al. HBO1 is required for the maintenance of leukaemia stem cells. *Nature*. 2020;577(7789):266-270.
13. Arany Z, Newsome D, Oldread E, Livingston DM, Eckner R. A family of transcriptional adaptor proteins targeted by the E1A oncoprotein. *Nature*. 1995;374(6517):81-84.
14. Goodman RH, Smolik S. CBP/p300 in cell growth, transformation, and development. *Genes Dev*. 2000;14(13):1553-1577.
15. Liu X, Wang L, Zhao K, et al. The structural basis of protein acetylation by the p300/CBP transcriptional coactivator. *Nature*. 2008;451(7180):846-850.
16. Weinert BT, Narita T, Satpathy S, et al. Time-Resolved Analysis Reveals Rapid Dynamics and Broad Scope of the CBP/p300 Acetylome. *Cell*. 2018;174(1):231-244 e212.
17. Narita T, Ito S, Higashijima Y, et al. Enhancers are activated by p300/CBP activity-dependent PIC assembly, RNAPII recruitment, and pause release. *Mol Cell*. 2021;81(10):2166-2182 e2166.
18. Kasper LH, Boussouar F, Ney PA, et al. A transcription-factor-binding surface of coactivator p300 is required for haematopoiesis. *Nature*. 2002;419(6908):738-743.
19. Reynoird N, Schwartz BE, Delvecchio M, et al. Oncogenesis by sequestration of CBP/p300 in transcriptionally inactive hyperacetylated chromatin domains. *EMBO J*. 2010;29(17):2943-2952.
20. Zhang Y, Xue Y, Shi J, et al. The ZZ domain of p300 mediates specificity of the adjacent HAT domain for histone H3. *Nat Struct Mol Biol*. 2018;25(9):841-849.
21. Dhalluin C, Carlson JE, Zeng L, He C, Aggarwal AK, Zhou MM. Structure and ligand of a histone acetyltransferase bromodomain. *Nature*. 1999;399(6735):491-496.
22. Lasko LM, Jakob CG, Edalji RP, et al. Discovery of a selective catalytic p300/CBP inhibitor that targets lineage-specific tumours. *Nature*. 2017;550(7674):128-132.
23. Michaelides MR, Kluge A, Patane M, et al. Discovery of Spiro Oxazolidinediones as Selective, Orally Bioavailable Inhibitors of p300/CBP Histone Acetyltransferases. *ACS Med Chem Lett*. 2018;9(1):28-33.
24. Picaud S, Fedorov O, Thanasopoulou A, et al. Generation of a Selective Small Molecule Inhibitor of the CBP/p300 Bromodomain for Leukemia Therapy. *Cancer Res*. 2015;75(23):5106-5119.
25. Nicosia L, Spencer GJ, Brooks N, et al. Therapeutic targeting of EP300/CBP by bromodomain inhibition in hematologic malignancies. *Cancer Cell*. 2023;41(12):2136-2153 e2113.
26. Welti J, Sharp A, Brooks N, et al. Targeting the p300/CBP Axis in Lethal Prostate Cancer. *Cancer Discov*. 2021;11(5):1118-1137.

27. Allis CD, Jenuwein T. The molecular hallmarks of epigenetic control. *Nat Rev Genet*. 2016;17(8):487-500.
28. Assi SA, Imperato MR, Coleman DJL, et al. Subtype-specific regulatory network rewiring in acute myeloid leukemia. *Nat Genet*. 2019;51(1):151-162.
29. Roe JS, Mercan F, Rivera K, Pappin DJ, Vakoc CR. BET Bromodomain Inhibition Suppresses the Function of Hematopoietic Transcription Factors in Acute Myeloid Leukemia. *Mol Cell*. 2015;58(6):1028-1039.
30. Long HK, Prescott SL, Wysocka J. Ever-Changing Landscapes: Transcriptional Enhancers in Development and Evolution. *Cell*. 2016;167(5):1170-1187.
31. Shah V, Giotopoulos G, Osaki H, et al. Acute resistance to BET inhibitors remodels compensatory transcriptional programs via p300 coactivation. *Blood*. 2025;145(7):748-764.
32. Smeenk L, Ottema S, Mulet-Lazaro R, et al. Selective Requirement of MYB for Oncogenic Hyperactivation of a Translocated Enhancer in Leukemia. *Cancer Discov*. 2021;11(11):2868-2883.
33. Tie F, Banerjee R, Stratton CA, et al. CBP-mediated acetylation of histone H3 lysine 27 antagonizes Drosophila Polycomb silencing. *Development*. 2009;136(18):3131-3141.
34. Creyghton MP, Cheng AW, Welstead GG, et al. Histone H3K27ac separates active from poised enhancers and predicts developmental state. *Proc Natl Acad Sci U S A*. 2010;107(50):21931-21936.
35. Sankar A, Mohammad F, Sundaramurthy AK, et al. Histone editing elucidates the functional roles of H3K27 methylation and acetylation in mammals. *Nat Genet*. 2022;54(6):754-760.
36. Wilson JE, Patel G, Patel C, et al. Discovery of CPI-1612: A Potent, Selective, and Orally Bioavailable EP300/CBP Histone Acetyltransferase Inhibitor. *ACS Med Chem Lett*. 2020;11(6):1324-1329.
37. Vannam R, Sayilgan J, Ojeda S, et al. Targeted degradation of the enhancer lysine acetyltransferases CBP and p300. *Cell Chem Biol*. 2021;28(4):503-514 e512.
38. Yun H, Narayan N, Vohra S, et al. Mutational synergy during leukemia induction remodels chromatin accessibility, histone modifications and three-dimensional DNA topology to alter gene expression. *Nat Genet*. 2021;53(10):1443-1455.
39. Mupo A, Celani L, Dovey O, et al. A powerful molecular synergy between mutant Nucleophosmin and Flt3-ITD drives acute myeloid leukemia in mice. *Leukemia*. 2013;27(9):1917-1920.
40. Kiladjian JJ, Klade C, Georgiev P, et al. Long-term outcomes of polycythemia vera patients treated with ropeginterferon Alfa-2b. *Leukemia*. 2022;36(5):1408-1411.
41. Mascarenhas J, Kosiorek HE, Prchal JT, et al. A randomized phase 3 trial of interferon-alpha vs hydroxyurea in polycythemia vera and essential thrombocythemia. *Blood*. 2022;139(19):2931-2941.
42. Gisslinger H, Klade C, Georgiev P, et al. Ropeginterferon alfa-2b versus standard therapy for polycythaemia vera (PROUD-PV and CONTINUATION-PV): a randomised, non-inferiority, phase 3 trial and its extension study. *Lancet Haematol*. 2020;7(3):e196-e208.
43. Kiladjian JJ, Cassinat B, Chevret S, et al. Pegylated interferon-alfa-2a induces complete hematologic and molecular responses with low toxicity in polycythemia vera. *Blood*. 2008;112(8):3065-3072.
44. Abruzzese E, Chelysheva E. How I Manage Chronic Myeloid Leukemia During Pregnancy. *Blood*. 2025.

45. Catalano L, Majolino I, Musto P, et al. Alpha interferon in the treatment of chronic myelomonocytic leukemia. *Haematologica*. 1989;74(6):577-581.
46. Nand S, Ellis T, Messmore H, Fisher SG, Gaynor E, Fisher RI. Phase II trial of recombinant human interferon alpha in myelodysplastic syndromes. *Leukemia*. 1992;6(3):220-223.
47. Anguille S, Lion E, Willemen Y, Van Tendeloo VF, Berneman ZN, Smits EL. Interferon-alpha in acute myeloid leukemia: an old drug revisited. *Leukemia*. 2011;25(5):739-748.
48. Hunt G, Boija A, Mannervik M. p300/CBP sustains Polycomb silencing by non-enzymatic functions. *Mol Cell*. 2022;82(19):3580-3597 e3589.
49. Ferrie JJ, Karr JP, Graham TGW, et al. p300 is an obligate integrator of combinatorial transcription factor inputs. *Mol Cell*. 2024;84(2):234-243 e234.
50. Zandarashvili L, Langelier MF, Velagapudi UK, et al. Structural basis for allosteric PARP-1 retention on DNA breaks. *Science*. 2020;368(6486).
51. Bhattacharya S, Eckner R, Grossman S, et al. Cooperation of Stat2 and p300/CBP in signalling induced by interferon-alpha. *Nature*. 1996;383(6598):344-347.
52. Paulson M, Pisharody S, Pan L, Guadagno S, Mui AL, Levy DE. Stat protein transactivation domains recruit p300/CBP through widely divergent sequences. *J Biol Chem*. 1999;274(36):25343-25349.
53. Wojciak JM, Martinez-Yamout MA, Dyson HJ, Wright PE. Structural basis for recruitment of CBP/p300 coactivators by STAT1 and STAT2 transactivation domains. *EMBO J*. 2009;28(7):948-958.
54. Ellegast JM, Alexe G, Hamze A, et al. Unleashing Cell-Intrinsic Inflammation as a Strategy to Kill AML Blasts. *Cancer Discov*. 2022;12(7):1760-1781.
55. Kawasaki H, Eckner R, Yao TP, et al. Distinct roles of the co-activators p300 and CBP in retinoic-acid-induced F9-cell differentiation. *Nature*. 1998;393(6682):284-289.
56. Ramos YF, Hestand MS, Verlaan M, et al. Genome-wide assessment of differential roles for p300 and CBP in transcription regulation. *Nucleic Acids Res*. 2010;38(16):5396-5408.
57. Martire S, Nguyen J, Sundaresan A, Banaszynski LA. Differential contribution of p300 and CBP to regulatory element acetylation in mESCs. *BMC Mol Cell Biol*. 2020;21(1):55.

Figure legends

Figure 1. Inhibition of p300/CREBBP lysine acetyltransferase induces interferon-stimulated gene expression

A. Uniform manifold approximation and projection (UMAP) plot of scRNA-seq expression profiles in MOLM-13 cells treated with KATi or DMSO for 24hr. Data represent 5842 cells (DMSO) and 9432 cells (KATi). ISG scores were calculated as the average log-normalized expression of the 26 most upregulated ISGs upon KATi treatment (*CXCL10, DDX60, EIF2AK2, EPSTI1, HELZ2, IFI16, IFI27, IFI44, IFI44L, IFIH1, IFIT1, IFIT2, IFIT3, IRF9, MX1, MX2, OAS1, OAS2, OAS3, OASL, PARP12, PARP14, RSAD2, SAMD9L, STAT1, XAF1*), and scaled to z-scores using the ScaleData function (RNA assay) in Seurat v5.2.1 before plotting.

B-C. Gene set enrichment analysis (GSEA) of scRNA-seq data from MOLM-13 (B) and OCI-AML3 (C) cells treated with KATi or DMSO for 24hr. Differential expression analysis was performed on log-normalized counts using the FindMarkers function in Seurat (RNA assay, Wilcoxon rank-sum test, adjusted p <0.05). GSEA was performed using the fgsea R package (v1.28.0) against MSigDB Hallmark gene sets (v2023.1.Hs), with 10,000 permutations. NES, normalized enrichment score.

D. UMAPs showing log-normalized expression of four representative ISGs (*CXCL10, STAT1, IFIT3, OAS3)* in MOLM-13 cells treated with KATi or DMSO for 24hr. Data are from the same scRNA-seq dataset as in panel 1A.

E. GSEA of SILAC-based quantitative proteomics from MOLM-13 cells treated with KATi or DMSO for 24hr (n = 3 biological replicates per condition). Proteins were quantified by mass spectrometry and differential expression was assessed using limma (v3.44.3). Ranked log2 fold-change values were analyzed with fgsea against MSigDB Hallmark gene sets, using 10,000 permutations, minSize = 15, maxSize = 500 and significance threshold FDR q < 0.05.

F. Lollipop plot showing the top 25 proteins with increased expression relative to baseline from the same dataset as 1E. ISGs are highlighted in red.

G. Real-time quantitative PCR (qPCR) analysis of *CXCL10* expression in 14 AML cell lines treated with KATi or DMSO for 24hr (n = 3 biological replicates and mean). Cell lines with high *CXCL10* induction following KATi treatment are highlighted in red and designated as “ISG high”.

H. TF dependencies in ISG high versus ISG low AML cell lines. The 14 AML cell lines from panel 1G were intersected with the Cancer Dependency Map (DepMap) CRISPR–Cas9 dependency dataset (Chronos, 25Q2). Thirteen cell lines were present in the dataset and further annotated by phenotype: MV411 (monocytic, high), SKNO1 (granulocytic, low), HEL (erythroid, low), NB4 (promyelocytic, low), OCI-AML2 (myelomonocytic, high), MOLM-13 (monocytic, high), OCI-AML3 (myelomonocytic, high), MOLM-14 (monocytic, high), U937 (monocytic, high), TF-1 (erythroid, high), KASUMI-1 (granulocytic, low), NOMO-1 (monocytic, low) and THP-1 (monocytic, high). Significant dependencies were identified by two-class comparison in DepMap, calculating the mean dependency score difference (ISG high minus ISG low) and associated p-values. TFs were then prioritized based on effect size (absolute mean difference ≥ 0.5). To assess combinatorial importance, scaled dependency scores for “trusted” TFs were used to generate all possible combinations (1-6 TFs) and combination performance was ranked by the difference in mean dependency between ISG-high and ISG-low cell lines. Results are displayed as dependency network of TFs significantly enriched in ISG-high lines. Also see Figure S1B.

I. Dose-dependent induction of *CXCL10* expression following 24hr treatment with KATi or CPI-1612 at the indicated concentrations versus DMSO control in MOLM-13 and OCI-AML3 cells. *CXCL10* mRNA levels were quantified by RT-qPCR, normalized to *GAPDH* expression and shown as fold change relative to DMSO. Shown are n = 3 independent biological replicates and means. Significance for each dose versus DMSO was assessed using a one-tailed Student’s t-test (treatment > DMSO) with Bonferroni and Benjamini-Hochberg FDR correction; reported p-values are Bonferroni-corrected.

J. Schematic model depicting STAT1 as a mediator of ISG induction downstream of p300/CREBBP KAT inhibition. This model provided the rationale for generating an inducible *STAT1* knockdown system to assess the impact of STAT1 loss on treatment efficacy and *CXCL10* induction after KATi.

K. RT-qPCR of *CXCL10* in MOLM-13 and OCI-AML3 cells after doxycycline-inducible *STAT1* knockdown (two independent shRNAs) or scramble control (shSCR), with or without KATi for 24hr. mRNA was normalized to *GAPDH* and shown as fold change relative to DMSO. Data represent the mean of n = 3 independent biological replicates. Significance for each comparison was assessed using one-tailed t-tests with prespecified direction (e.g., KATi + shSTAT1 < KATi + shSCR), with Bonferroni and Benjamini-Hochberg FDR correction for multiple comparisons; reported p-values are Bonferroni-corrected.

L. ATP-based luminescence signal curves (CellTiter-Glo) for MOLM-13 and OCI-AML3 cells treated with graded doses of KATi following *STAT1* knockdown (two independent shRNAs) or scramble (shSCR) control. Data represent the mean of n = 3 independent biological replicates. For each dose, differences between shSTAT1 and shSCR were tested using one-tailed t-tests (hypothesis: shSTAT1 < scramble), with Bonferroni and Benjamini-Hochberg FDR correction; reported p-values are Bonferroni-corrected. Analysis was measured at 72hr of treatment.

Figure 2. ISG release is associated with p300/CREBBP catalytic inhibition in the presence of an intact scaffolding/signal-integrating platform

A. Schematic representation of the three strategies targeting p300/CREBBP: degradation (Deg), bromodomain inhibition (BRDi) and catalytic domain inhibition (KATi).

B. Dose-response curves showing ATP-based luminescence signal (CellTiter-Glo) of 8 AML cell lines (6 ISG high, 2 ISG low from Figure 1G) treated at the indicated concentrations. N = 3 biological replicates; data are normalized to DMSO controls and shown as mean ± s.d.

C-D. Dot plots of GSEA (MSigDB Hallmark gene sets; R msigdbr package) from SLAM-seq data in MOLM-13 cells (n = 3) treated for 2, 12 or 24hr versus DMSO, which was considered timepoint zero. Analyses were performed separately for nascent RNA and total RNA. Gene sets are grouped by direction of change: decreased (C) and increased (D) transcription and subsequent mRNA accumulation. Dot size represents normalized enrichment score (NES); dot color represents −log10(adjusted p-value, < 0.01). Deg was used at 250 nM, BRDi at 500 nM and KATi at 1000 nM.

E. ISG scores based on nascent RNA from SLAM-seq in MOLM-13 cells (n = 3) treated with Deg, BRDi or KATi versus DMSO for the indicated time points. ISG genes as defined in Figure 1A. Deg was used at 250 nM, BRDi at 500 nM and KATi at 1000 nM.

F. Log2 fold changes of *CXCL10* expression relative to DMSO at 4, 12, 20 and 24hr following KATi (1000 nM), and directly at 24hr following Deg (250 nM) or BRDi (500 nM) (n = 3; data represent mean ± s.d.).

G-H. Log2 fold changes of *CXCL10* expression relative to DMSO 24hr after KATi (1000 nM), with Deg (250 nM) (**G**) or BRDi (500 nM) (**H**) administered sequentially at 4, 12 or 20hr post-KATi initiation

and each time measured at 24hr (n = 3; data represent mean ± s.d.). For each plot, a one-tailed Student's *t*-test was performed comparing the 24hr sequential treatment condition to the last time point prior to the addition of either Deg or BRDi.

Figure 3. KAT inhibition retains p300/CREBBP at IRF motif-enriched, immune regulatory elements

A. Schematic representation of the comparative deconvolution of p300/CREBBP-associated chromatin functions following KAT inhibition, encompassing chromatin interactors (RIME), acetylation targets (acetyl-proteomics), TF motif enrichment analysis and binding dynamics at target sites.

B. RIME comparing p300 versus IgG control in MOLM-13 and OCI-AML3 cells (n = 4 (MOLM-13) and n = 3 (OCI-AML3) per group). Cells (50×10^6 per replicate) were formaldehyde-crosslinked, immunoprecipitated with anti-p300 or IgG isotype control and subjected to LC-MS/MS. Volcano plots depict significantly enriched interactors based on a cut-off of adjusted p-value <0.05 and log2 fold change ≥ 1.

C. RIME of the BAF complex component ARID1A versus IgG control in MOLM-13 cells (n = 4 biological replicates) processed and analyzed as in **(B)**.

D. SILAC-based acetyl-proteomics identifying p300/CREBBP-dependent acetylation sites after catalytic inhibition. MOLM-13 and OCI-AML3 cells were cultured in heavy/light SILAC media, treated with KATi or DMSO for 24hr and analyzed by LC–MS/MS (n = 3 biological replicates per cell line). Data from both cell lines were merged and only lysine residues detected in at least 4 out of 6 total replicates were included. Acetylation scores were calculated as the log2 fold change (KATi/DMSO); a more negative score indicates a stronger reduction in acetylation upon KAT inhibition and thus greater acetylation by the p300/CREBBP KAT domain. Highlighted genes represent selected chromatin regulators and TFs of interest.

E-F. De novo motif enrichment analysis of p300- and CREBBP-bound regions. ChIP-seq was performed in MOLM-13 and OCI-AML3 cells using antibodies against p300 or CREBBP following 24 h treatment with either DMSO or KATi (n = 2 biological replicates per condition). Peak calling was performed separately for each replicate and condition, and binding site "catalogs" were generated for p300, CREBBP and their intersection ("common sites") by merging peaks across replicates and treatments. De novo motif discovery was performed on each catalog using HOMER v4.11.1 (findMotifsGenome.pl) with default parameters and matched background sequences. Plotted are the motif enrichment scores and –log10 p-values for the most significant and recurrent motif families across conditions: ETS, CEBP, bZIP, RUNX, IRF, MEF, MYB, HOX and CTCF (CTCF enrichment observed only in CREBBP ChIP-seq). Panel (**E)** shows results for individual p300 and CREBBP catalogs; Panel (**F)** shows results for common binding sites.

G. Proposed p300/CREBBP acetyl-interactome model integrating evidence from RIME, SILAC-based acetyl-proteomics and ChIP-seq-based motif co-occupancy. Nodes denote candidate acetyl-interactors; dark red indicates support from ≥2 assays, light red from a single assay. Edges represent predicted functional associations from STRING-db.

H. Heatmap (tornado plot) of ChIP-seq signal (±1 kb around peak centers) for p300 and CREBBP in MOLM-13 and OCI-AML3 cells at common p300/CREBBP co-bound peaks (peak union across KATi and DMSO as defined in Figure 3E, with 18,175 peaks in MOLM-13 and 14,914 peaks in OCI-AML3) after 24hr treatment with KATi or DMSO. Both proteins show increased occupancy at a subset of loci after KATi (retained regions). The top 10% most strongly retained regions (marked with a red dashed line) were defined as the top decile of these co-bound peaks ranked by the increase in normalized ChIP-Seq signal under KATi versus DMSO (delta signal) and were used for analyses in panels **I-K**.

I. Positional annotation of the top 10% retained common binding sites. Promoters were defined as −5 kb to +2.5 kb relative to the transcription start site (TSS); all other regions were classified as enhancers/other.

J. Overrepresentation analysis of the top three enriched Gene Ontology (GO) Biological Process terms for the top 10% most strongly retained p300/CREBBP common-binding regions in MOLM-13 and OCI-AML3 cells after KATi treatment. Analysis was performed using GREAT; results are shown separately for each cell line. Metrics include Binom_FDR_QVal and Binom_Region_Set_Coverage.

K. De novo motif enrichment analysis at the top 10% most retained p300-, CREBBP- and common-binding sites after KATi versus DMSO in MOLM-13 (upper) and OCI-AML3 (lower) cells. Plotted are enrichment scores and −log10(p-value) for the most significant motifs.

Figure 4. Inhibition of p300/CREBBP catalytic activity promotes combinatorial TF assembly and transcription at IRF motif-marked regulatory sites

A. Differential PRO-Seq signal in MOLM-13 cells after KATi versus DMSO. Differential expression was assessed using DiffBind; significant transcriptional changes were defined as adjusted $p < 0.05$. Labels indicate exemplary ISGs with significantly increased transcription after KATi treatment.

B. Binding of acetyl-interactome subunits p300, CREBBP, MEF2D, IRF8, CEBPA, CEBPB, ARID1A, PU.1, RUNX1, FLI1 and IRF2BP2, as well as histone marks H3K27ac and H3K27me3, in MOLM-13 cells at PRO-Seq-defined regions with significantly increased (red) or decreased (blue) transcription after KATi versus DMSO. ChIP-seq signal was quantified using the spline algorithm in ngs.plot (v2.61) and the median signal around each region was used to generate a binding score. Each dot represents the ratio of KATi/DMSO for the corresponding biological replicate of a given target. Statistical significance reflects the difference in score ratios between increased- and decreased-transcription regions, determined by two-tailed Student's t-test ($p < 0.0001$).

C. Binding of p300, CREBBP, MEF2D, SMARCA4, CEBPA, CEBPB, ARID1A, PU.1, RUNX1, FLI1 and IRF2BP2 in OCI-AML3 cells at PRO-Seq-defined regions with significantly increased (red) or decreased (blue) transcription after KATi versus DMSO, using differential transcription calls from MOLM-13 cells (Figure 4A). ChIP-seq signal was quantified using the spline algorithm in ngs.plot and the median signal around each region was used to generate a binding score. Each dot represents the ratio of KATi/DMSO for the corresponding biological replicate of a given target. Statistical significance reflects the difference in

score ratios between increased- and decreased-transcription regions, determined by two-tailed Student's t-test ($p < 0.0001$).

D. De novo motif enrichment analysis at transcriptionally decreased PRO-Seq regions (KATi/DMSO), corresponding to the 1547 down regions shown in Figure 4A. Enrichment scores and -log10(p-value) are plotted for the most significantly enriched motifs.

E. Binding of the indicated acetyl-interactome subunits in MOLM-13 cells at PRO-Seq-defined regions with significantly decreased transcription and containing motifs for MEF (left), MYB (middle) or ETS (right) TFs after KATi versus DMSO. ChIP-seq signal was quantified using the spline algorithm in ngs.plot and the median signal around each region was used to calculate a binding score. Scores for each target were averaged across biological replicates (n = 2) and expressed as the KATi/DMSO ratio for each region type.

F. De novo motif enrichment analysis at transcriptionally increased PRO–Seq regions (KATi/DMSO), corresponding to the 2971 up regions shown in Figure **4A**. Enrichment scores and -log10(p-value) are plotted for the most significantly enriched motifs.

G. Binding of the indicated acetyl-interactome subunits in MOLM-13 cells at PRO-Seq-defined regions with significantly increased transcription and containing motifs for IRF (left), KLF (middle) or ETS (right) TFs after KATi versus DMSO. ChIP-seq signal was quantified using the spline algorithm in ngs.plot and the median signal around each region was used to calculate a binding score. Scores for each target were averaged across biological replicates (n = 2) and expressed as the KATi/DMSO ratio for each region type.

H. PRO-seq and ChIP-seq tracks for p300/CREBBP acetyl-interactome subunits and H3K27ac at exemplar loci. **Left:** Loci with decreased PRO-seq signal and MEF/ETS_down/MYB motif enrichment (*CST7, HES1, ADGRG3*). **Right:** Loci with increased PRO-seq signal and IRF motif enrichment (*IFIT2, IFIT3, OAS2*). IGV tracks show data from MOLM-13 cells treated with DMSO or KATi; for the H3K27ac tracks, additional conditions include Deg (4hr) and KATi followed by Deg during the final 4hr of the 24hr treatment.

I. Matched ChIP-qPCR for CREBBP and H3K27ac at the *IFIT3* promoter showing concordant retention/accumulation upon KATi and reversal by late Deg addition. Data represent n = 3 biological replicates.

J. Left: Average profiles of H3K27ac at MEF motif-enriched sites with decreased transcription (left panels) and at IRF motif-enriched sites with increased transcription (right panels), comparing DMSO vs Deg_4hr (top), DMSO vs KATi_24hr (middle), and DMSO vs KATi_24hr + lateDeg_4hr (bottom).

Figure 5. Functional deconvolution of the p300/CREBBP acetyl-Interactome links ISG induction to combinatorial TF integrity

A. Schematic representation of the functional genomics approaches used to assess the individual contributions of p300/CREBBP acetyl-interactome subunits to KATi-induced cytotoxicity and, separately,

to KATi-induced ISG expression. **Left panel:** genome-wide CRISPR-Cas9 dropout screen (Brunello library) in KATi- versus DMSO-treated cells. **Right panel:** PERTURB-Seq with a custom sgRNA library targeting the p300/CREBBP acetyl-interactome, followed by single-cell RNA-seq in KATi- and DMSO-treated cells.

B–C. Genome-wide CRISPR-Cas9 dropout screens in MOLM-13 cells transduced with the Brunello sgRNA library and treated with **(B)** KATi versus DMSO or **(C)** BRDi versus DMSO at the respective IC50 concentrations for 48hr. Cells were harvested 14 days post-transduction and sgRNA abundance was quantified by high-throughput sequencing. Essentiality scores were calculated using the MaGeCK MLE algorithm, with Z-scores and p-values derived from differences in essentiality between treatment and control. Replicates (n = 2 for KATi, n = 2 for BRDi and n = 4 pooled DMSO controls (2 from each treatment comparison)) were analyzed jointly; significance was defined as $p < 0.05$.

D. Lollipop plot showing guide-level differences in ISG expression from a PERTURB-seq screen 24hr after KATi treatment. The y-axis indicates the difference in mean ISG score for each sgRNA relative to the mean score of non-targeting control guides (controls not shown). Negative values indicate reduced ISG induction; positive values indicate increased induction. Each point represents a unique sgRNA (n = 20 for *p300* and *CREBBP*, n = 8 for other target genes). Horizontal dashed lines mark two-tailed z-score thresholds (±1.96 ≈ p = 0.05; ±2.58 ≈ p = 0.01, unadjusted). Statistical significance was calculated from guide-level differences relative to non-targeting controls, with p-values adjusted for multiple testing using the Benjamini-Hochberg method.

E. Representative Zero Interaction Potency (ZIP) synergy scores in MOLM-13 and OCI-AML3 cells treated with KATi in combination with the BRG1 degrader ACBI1 across varying dose matrices (n = 3). Scores below -10 indicate antagonistic interactions. Interaction scores were calculated from ATP-based luminescence (CellTiter-Glo).

F. Schematic illustration proposing that, in addition to the KATi-induced increase in combinatorial TF binding, new TFs or co-regulators may gain regulatory access to induce ISG expression.

G. RIME of the BAF complex component ARID1A in MOLM-13 cells treated with KATi or DMSO for 24hr (n = 4). Upon KATi, ARID1A acquired new interactions with positive regulators of ISG expression, including STAT1, MX1 and IFI16.

H. Average STAT1 ChIP-seq binding profiles (n =2) in MOLM-13 cells treated with KATi or DMSO at PROSeq-defined regions with decreased transcription (containing MEF, MYB and ETS motifs) or increased transcription (containing IRF, KLF and ETS motifs).

I. Representative western blots for STAT1, phospho-STAT1 and β-tubulin (loading control) in MOLM-13 cells 24hr after KATi treatment at the indicated doses (shown is one of n = 3 representative blots).

J. Representative ChIP-seq and PROSeq tracks for the ISGs *OAS2*, *IFIT3* and *STAT1* in MOLM-13 cells treated with DMSO or KATi, including new STAT1 binding at these ISGs upon KATi treatment.

K. ChIP-qPCR for STAT1 binding at the *IFIT3* and *OAS2* loci in MOLM-13 cells treated with DMSO, KATi for 24hr or KATi for 24hr with late Deg addition (Deg during the final 4hr). Data represent n = 3 biological replicates.

L. ChIP-qPCR for CREBBP binding at the *IFIT3* and *OAS2* loci in MOLM-13 cells treated with DMSO (reference baseline) or KATi for 24hr, performed in three isogenic lines: doxycycline-induced scrambled shRNA (shSCR) and two independent STAT1 knockdown constructs. Data represent n = 3 biological replicates.

Figure 6. Exogenous Interferon-alpha enhances KATi-Induced ISG activation and apoptosis

A. Flow cytometry analysis of apoptosis (Annexin V/7-AAD staining, upper panel) and cell cycle distribution (lower panel) in MOLM-13 cells treated with KATi at indicated concentrations and time points. Data represent mean ± s.d. Statistical significance was determined by one-way ANOVA with Tukey's multiple comparisons test.

B. Representative May-Grünwald Giemsa staining of OCI-AML3 (upper panel) and MOLM-13 (lower panel) cells treated with KATi at indicated concentrations for 72hr (n=3). Scale bar, 150 µm; magnified insets (corner) show 20 x enlarged cells.

C. Flow cytometry analysis of CD11b (left) and CD14 (right) surface marker expression in MOLM-13 cells following KATi versus DMSO for 72 and 120hr. Data represent mean ± s.e.m. Statistical significance was determined by two-way ANOVA with uncorrected Fisher's LSD test.

D. Illustration of the expected enhancement of KATi-induced ISG expression upon addition of exogenous IFNa.

E. *CXCL10* mRNA expression in MOLM-13 and OCI-AML3 cells treated for 24hr with DMSO, IFNa (10 ng/mL), KATi (500 nM) and IFNa + KATi; or with S-S-CPI (10 nM), IFNa (10 ng/mL), CPI-1612 (10 nM) and IFNa + CPI-1612. Data represent mean ± s.d. Statistical analysis was performed using two-tailed Student's *t* test.

F. Representative Annexin V/7-AAD flow cytometry plots showing apoptosis in MOLM-13 cells after 72hr of treatment. The same doses were used as in Figure 6E.

G. *CXCL10* mRNA expression in high-ISG (top) and low-ISG (bottom) AML cell lines following treatment with DMSO, IFNa (10 ng/mL), KATi (500 nM) or IFNa + KATi for 24hr. Data represent mean ± s.d. Statistical analysis was performed by one-tailed Student's *t* test.

H.-I. Flow cytometry analysis of cell death and apoptosis in both high and low ISG cell lines treated with DMSO, IFNa (10 ng/mL), KATi (500 nM) and IFNa + KATi (**H**); or with S-S-CPI (10 nM), IFNa (10 ng/mL), CPI-1612 (10 nM) and IFNa + CPI-1612 (**I**) for 72hr. Data represent mean ± s.d. Statistical analysis was performed by two-tailed Student's *t* test.

J. Representative ZIP synergy scores for KATi + IFNa (left) or CPI-1612 + IFNa (right) in MOLM-13 (top) and OCI-AML3 (bottom) cells (n = 3). ZIP scores > 10 were considered synergistic.

Figure 7. KAT inhibition with interferon-alpha demonstrates efficacy *in-vivo* and *ex-vivo*

A. Kaplan-Meier survival curves of NSG mice (n=8 per group) engrafted with 1 x 10^6 MOLM-13 cells and treated with vehicle, recombinant human IFNa (1 x 10^6 U/kg), KATi (100 mg/kg) or IFNa + KATi starting one week after AML tail vein injection and continuing for 15 days (or less, in case of death events) post-transplant. p values were determined using log-rank (Mantel-Cox) test.

B. Flow cytometry analysis of human $CD45^+$ cells in peripheral blood (left) and spleen (right) from xenograft NSG mice treated with vehicle (n=5), IFNa (n=5), KATi (n=3) or IFNa + KATi (n=8) at the time of death. Data represent mean ± s.d. p values were determined by one-way ANOVA with Bonferroni's multiple comparisons test.

C. *Cxcl10* mRNA expression in murine *Npm1c/Flt3-ITD* AML cells treated for 24hr with DMSO, IFNa (low: 6250 U/mL; high: 25000 U/mL), KATi (low: 200 nM; high: 800 nM) or IFNa + KATi. Data represent mean ± s.d.

D. Representative ZIP synergy score of KATi + IFNa in murine *Npm1c/Flt3-ITD* AML cells (n=3). ZIP scores > 10 were considered synergistic.

E. Kaplan-Meier survival curves of C57BL/6 mice (n=6-7 per group) engrafted with 5 x 10^5 murine *Npm1c/Flt3-ITD* AML cells and treated with vehicle, recombinant murine IFNa (1 x 10^6 U/kg), KATi (100 mg/kg) or IFNa + KATi starting one week after AML tail vein injection and continuing for 15 days post-transplant. p values were determined using log-rank (Mantel-Cox) test.

F-I. *CXCL10* **(F),** *STAT1* **(G),** *OAS3* **(H)** and *IFIT3* **(I)** mRNA expression in primary mononuclear cells from CMML (n = 4) and AML (n = 7) patients treated with DMSO, IFNa (10 ng/mL), KATi (500 nM), or IFNa + KATi for 24hr. Data represent mean ± s.d.

J. ATP-based luminescence signal (CellTiter-Glo) of CMML (n=3) and AML (n=4) primary mononuclear cells treated with DMSO, IFNa (10 ng/mL), KATi (500 nM) or IFNa + KATi for 6 days. Data represent mean ± s.d.

K. Annexin V/7-AAD flow cytometry of CMML (n=1) and AML (n=4) primary mononuclear cells treated with DMSO, IFNa (10 ng/mL), KATi (500 nM) or IFNa + KATi for 5 days. Data represent mean ± s.d.

L. Quantification of colony-forming units in CMML primary mononuclear cells treated with DMSO, IFNa (10 ng/mL), KATi (500 nM) or IFNa + KATi for 7 days. Data represent the mean of two technical replicates.

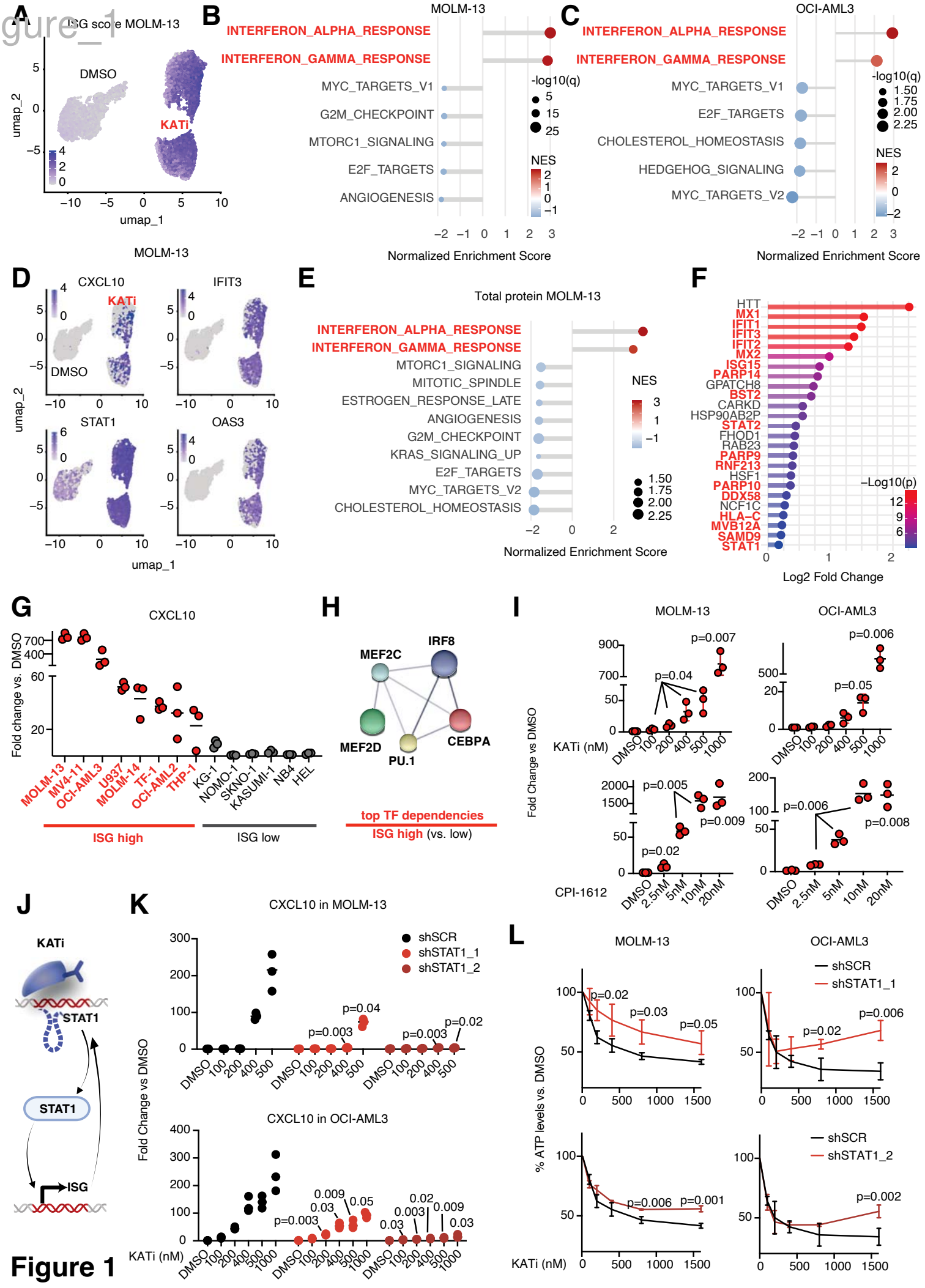
A
ISG score MOLM-13
DMSO
KATi
umap_1
umap_2
MOLM-13
B
MOLM-13
INTERFERON_ALPHA_RESPONSE
INTERFERON_GAMMA_RESPONSE
MYC_TARGETS_V1
G2M_CHECKPOINT
MTORC1_SIGNALING
E2F_TARGETS
ANGIOGENESIS
-log10(q)
NES
Normalized Enrichment Score
C
OCI-AML3
INTERFERON_ALPHA_RESPONSE
INTERFERON_GAMMA_RESPONSE
MYC_TARGETS_V1
E2F_TARGETS
CHOLESTEROL_HOMEOSTASIS
HEDGEHOG_SIGNALING
MYC_TARGETS_V2
-log10(q)
NES
Normalized Enrichment Score
D
CXCL10
IFIT3
STAT1
OAS3
KATi
DMSO
umap_1
umap_2
E
Total protein MOLM-13
INTERFERON_ALPHA_RESPONSE
INTERFERON_GAMMA_RESPONSE
MTORC1_SIGNALING
MITOTIC_SPINDLE
ESTROGEN_RESPONSE_LATE
ANGIOGENESIS
G2M_CHECKPOINT
KRAS_SIGNALING_UP
E2F_TARGETS
MYC_TARGETS_V2
CHOLESTEROL_HOMEOSTASIS
NES
Normalized Enrichment Score
F
HTT
MX1
IFIT1
IFIT3
IFIT2
MX2
ISG15
PARP14
GPATCH8
BST2
CARKD
HSP90AB2P
STAT2
FHOD1
RAB23
PARP9
RNF213
HSF1
PARP10
DDX58
NCF1C
HLA-C
MVB12A
SAMD9
STAT1
-Log10(p)
Log2 Fold Change
G
CXCL10
Fold change vs. DMSO
MOLM-13
MV4-11
OCI-AML3
U937
MOLM-14
TF-1
OCI-AML2
THP-1
KG-1
NOMO-1
SKNO-1
KASUMI-1
NB4
HEL
ISG high
ISG low
H
IRF8
MEF2C
MEF2D
CEBPA
PU.1
top TF dependencies
ISG high (vs. low)
I
MOLM-13
OCI-AML3
Fold Change vs DMSO
KATi (nM)
CPI-1612
p=0.007
p=0.04
p=0.006
p=0.05
p=0.005
p=0.009
p=0.02
p=0.008
J
KATi
STAT1
STAT1
ISG
K
CXCL10 in MOLM-13
shSCR
shSTAT1_1
shSTAT1_2
CXCL10 in OCI-AML3
Fold Change vs DMSO
KATi (nM)
L
MOLM-13
OCI-AML3
% ATP levels vs. DMSO
KATi (nM)
shSCR
shSTAT1_1
shSTAT1_2
p=0.02
p=0.03
p=0.05
p=0.006
p=0.001
p=0.002

Figure 1

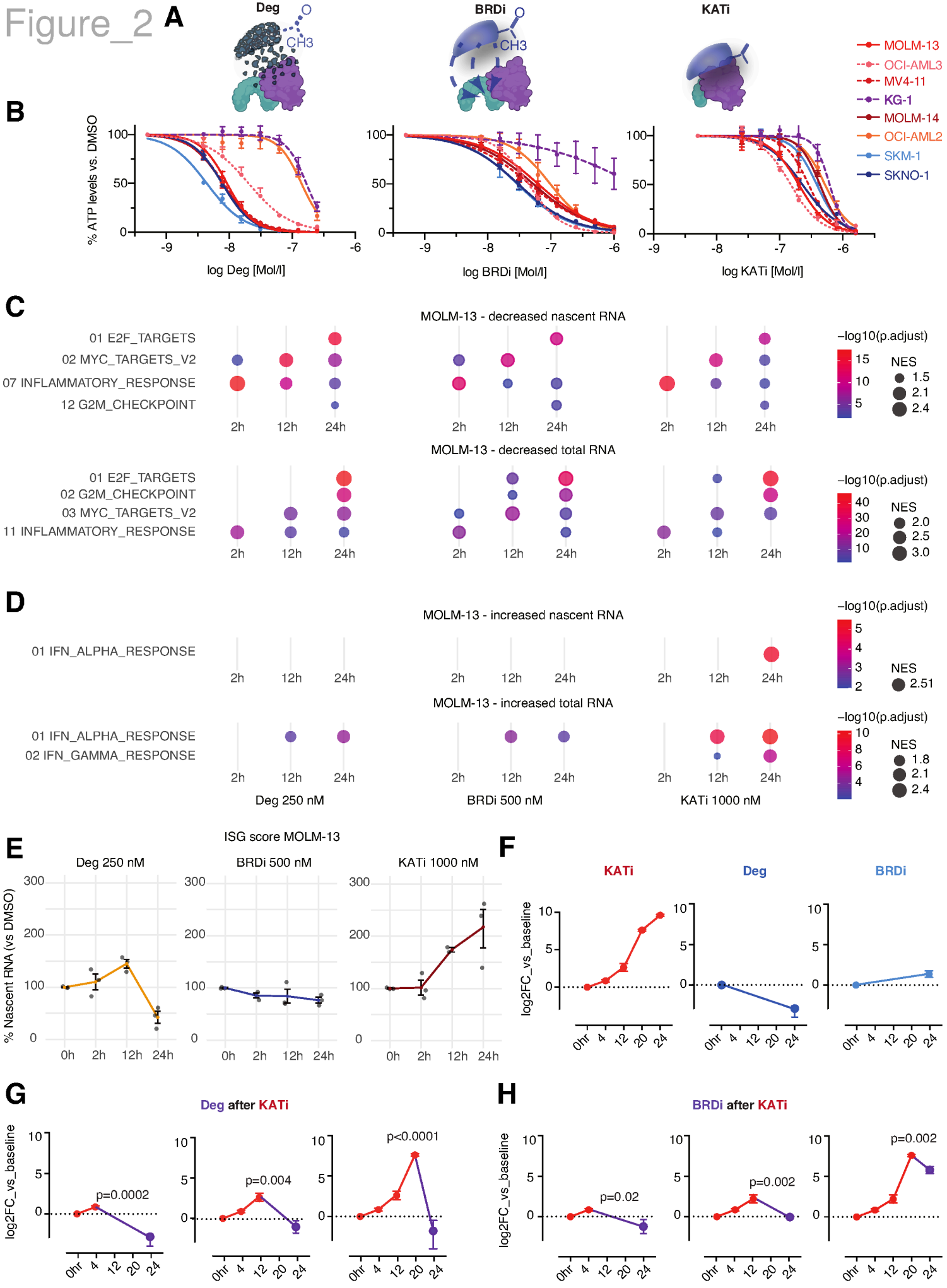
A
Deg
BRDi
KATi
CH3
O
MOLM-13
OCI-AML3
MV4-11
KG-1
MOLM-14
OCI-AML2
SKM-1
SKNO-1
B
% ATP levels vs. DMSO
log Deg [Mol/l]
log BRDi [Mol/l]
log KATi [Mol/l]
C
MOLM-13 - decreased nascent RNA
01 E2F_TARGETS
02 MYC_TARGETS_V2
07 INFLAMMATORY_RESPONSE
12 G2M_CHECKPOINT
MOLM-13 - decreased total RNA
01 E2F_TARGETS
02 G2M_CHECKPOINT
03 MYC_TARGETS_V2
11 INFLAMMATORY_RESPONSE
2h
12h
24h
−log10(p.adjust)
NES
D
MOLM-13 - increased nascent RNA
01 IFN_ALPHA_RESPONSE
MOLM-13 - increased total RNA
01 IFN_ALPHA_RESPONSE
02 IFN_GAMMA_RESPONSE
Deg 250 nM
BRDi 500 nM
KATi 1000 nM
E
ISG score MOLM-13
Deg 250 nM
BRDi 500 nM
KATi 1000 nM
% Nascent RNA (vs DMSO)
0h
2h
12h
24h
F
KATi
Deg
BRDi
log2FC_vs_baseline
0hr
4
12
20
24
G
Deg after KATi
p=0.0002
p=0.004
p<0.0001
H
BRDi after KATi
p=0.02
p=0.002
p=0.002

Figure 2

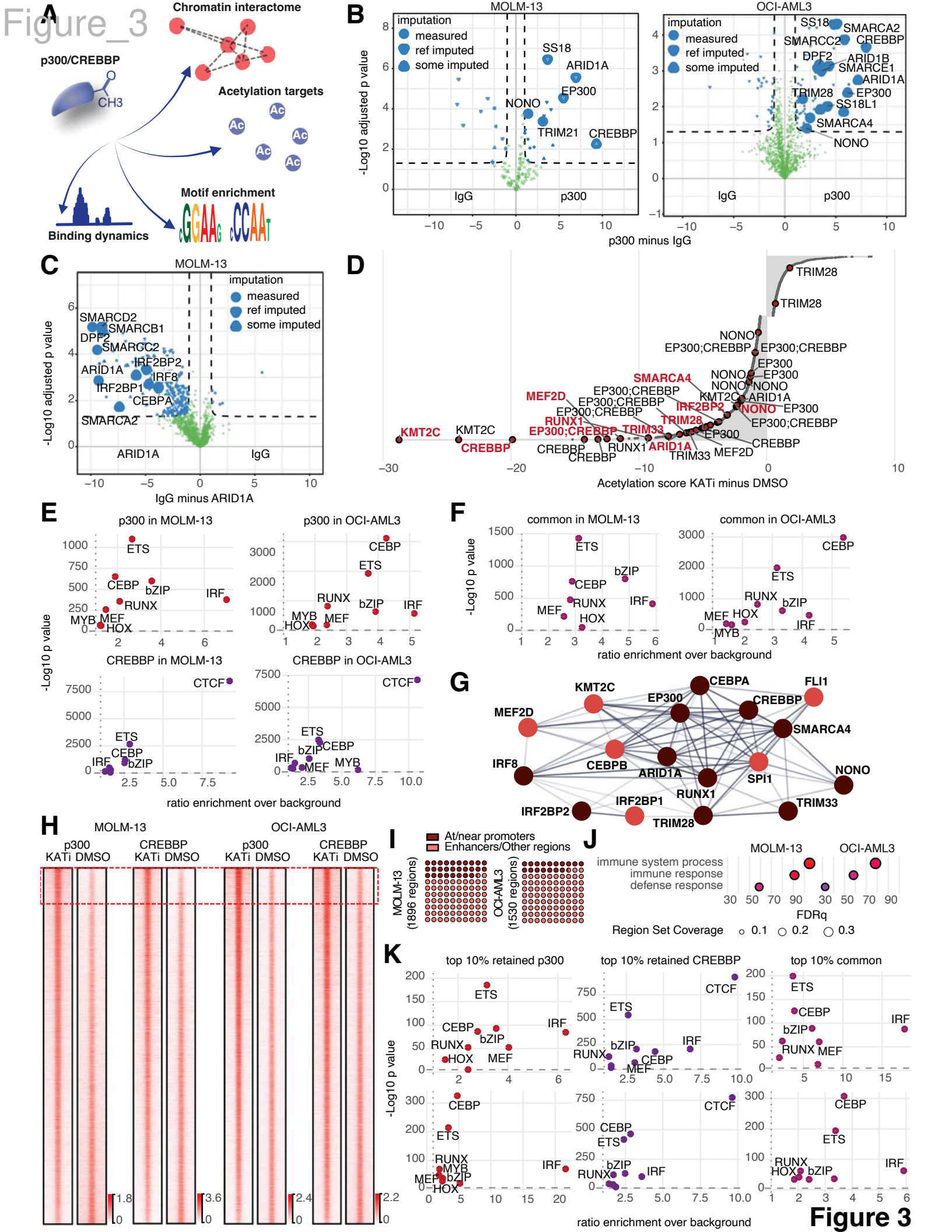
Figure_3
A
Chromatin interactome
p300/CREBBP
CH3
Acetylation targets
Ac
Motif enrichment
Binding dynamics
B
MOLM-13
OCI-AML3
imputation
measured
ref imputed
some imputed
-Log10 adjusted p value
SS18
ARID1A
EP300
NONO
TRIM21
CREBBP
SMARCA2
SMARCC2
DPF2
ARID1B
SMARCE1
TRIM28
SS18L1
SMARCA4
IgG
p300
p300 minus IgG
C
MOLM-13
SMARCD2
SMARCB1
DPF2
SMARCC2
ARID1A
IRF2BP2
IRF8
IRF2BP1
CEBPA
SMARCA2
IgG minus ARID1A
D
TRIM28
NONO
EP300;CREBBP
EP300
SMARCA4
MEF2D
KMT2C
CREBBP
RUNX1
TRIM33
ARID1A
TRIM28
IRF2BP2
Acetylation score KATi minus DMSO
E
p300 in MOLM-13
p300 in OCI-AML3
CREBBP in MOLM-13
CREBBP in OCI-AML3
ETS
CEBP
bZIP
RUNX
IRF
MYB
MEF
HOX
CTCF
-Log10 p value
ratio enrichment over background
F
common in MOLM-13
common in OCI-AML3
-Log10 p value
ratio enrichment over background
G
KMT2C
CEBPA
FLI1
EP300
CREBBP
MEF2D
SMARCA4
IRF8
CEBPB
ARID1A
SPI1
NONO
IRF2BP1
RUNX1
IRF2BP2
TRIM33
TRIM28
H
MOLM-13
OCI-AML3
p300
KATi DMSO
CREBBP
KATi DMSO
I
At/near promoters
Enhancers/Other regions
MOLM-13 (1896 regions)
OCI-AML3 (1530 regions)
J
MOLM-13
OCI-AML3
immune system process
immune response
defense response
FDRq
Region Set Coverage
0.1
0.2
0.3
K
top 10% retained p300
top 10% retained CREBBP
top 10% common
-Log10 p value
ratio enrichment over background
Figure 3

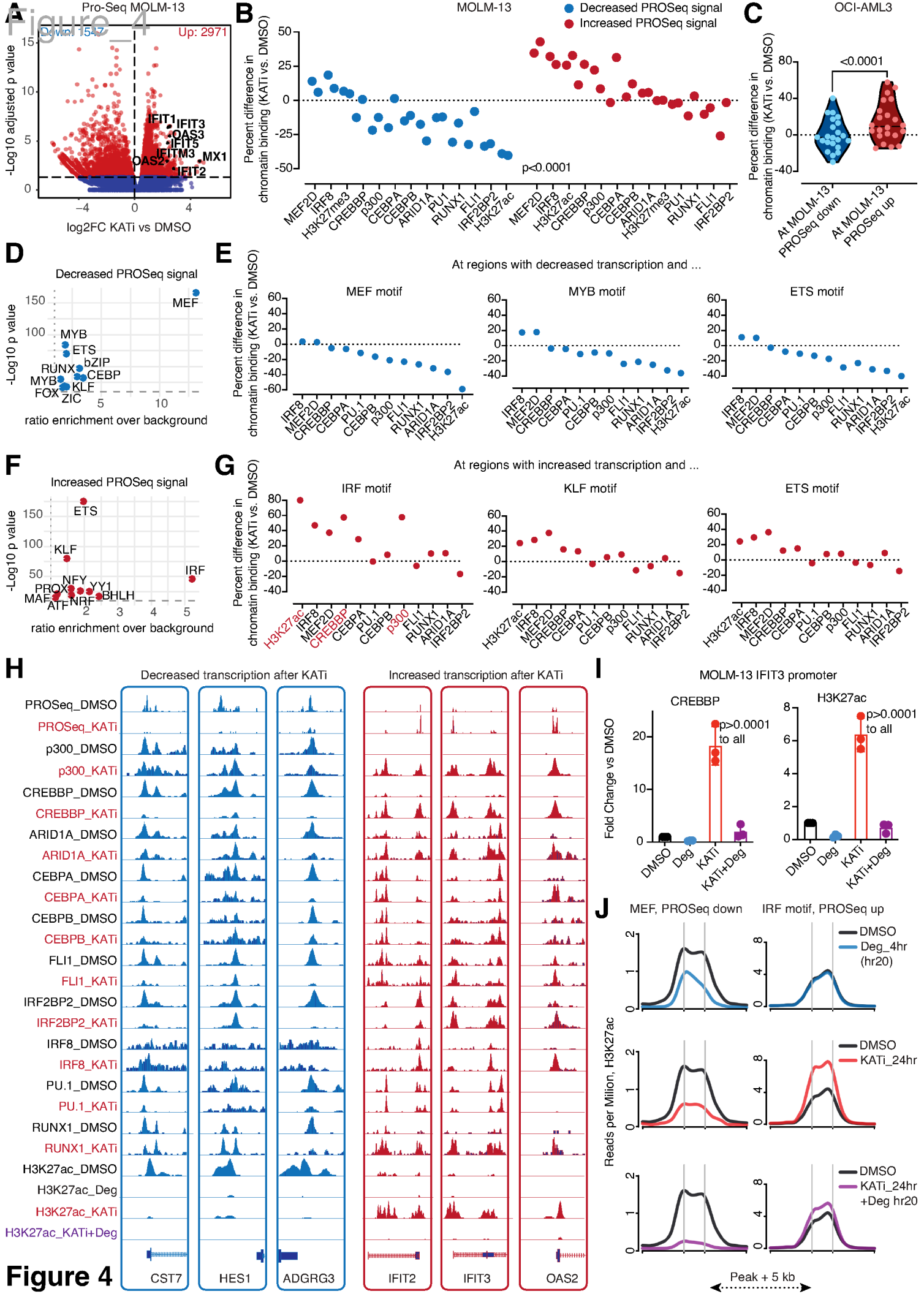
A
Pro-Seq MOLM-13
Down: 1547
Up: 2971
-Log10 adjusted p value
log2FC KATi vs DMSO
IFIT1
IFIT3
OAS3
IFIT5
IFITM3
MX1
OAS2
IFIT2
B
MOLM-13
Decreased PROSeq signal
Increased PROSeq signal
Percent difference in chromatin binding (KATi vs. DMSO)
p<0.0001
MEF2D
IRF8
H3K27me3
CREBBP
p300
CEBPA
CEBPB
ARID1A
PU1
RUNX1
FLI1
IRF2BP2
H3K27ac
C
OCI-AML3
<0.0001
At MOLM-13 PROSeq down
At MOLM-13 PROSeq up
D
Decreased PROSeq signal
-Log10 p value
MEF
MYB
ETS
RUNX
bZIP
CEBP
MYB
KLE
FOX
ZIC
ratio enrichment over background
E
At regions with decreased transcription and ...
MEF motif
MYB motif
ETS motif
F
Increased PROSeq signal
ETS
KLF
IRF
NFY
YY1
PROX
MAF
ATF
NRF
BHLH
G
At regions with increased transcription and ...
IRF motif
KLF motif
ETS motif
H
Decreased transcription after KATi
Increased transcription after KATi
PROSeq_DMSO
PROSeq_KATi
p300_DMSO
p300_KATi
CREBBP_DMSO
CREBBP_KATi
ARID1A_DMSO
ARID1A_KATi
CEBPA_DMSO
CEBPA_KATi
CEBPB_DMSO
CEBPB_KATi
FLI1_DMSO
FLI1_KATi
IRF2BP2_DMSO
IRF2BP2_KATi
IRF8_DMSO
IRF8_KATi
PU.1_DMSO
PU.1_KATi
RUNX1_DMSO
RUNX1_KATi
H3K27ac_DMSO
H3K27ac_Deg
H3K27ac_KATi
H3K27ac_KATi+Deg
CST7
HES1
ADGRG3
IFIT2
IFIT3
OAS2
I
MOLM-13 IFIT3 promoter
CREBBP
H3K27ac
Fold Change vs DMSO
p>0.0001 to all
DMSO
Deg
KATi
KATi+Deg
J
MEF, PROSeq down
IRF motif, PROSeq up
Reads per Million, H3K27ac
DMSO
Deg_4hr (hr20)
KATi_24hr
KATi_24hr +Deg hr20
Peak + 5 kb

Figure 4

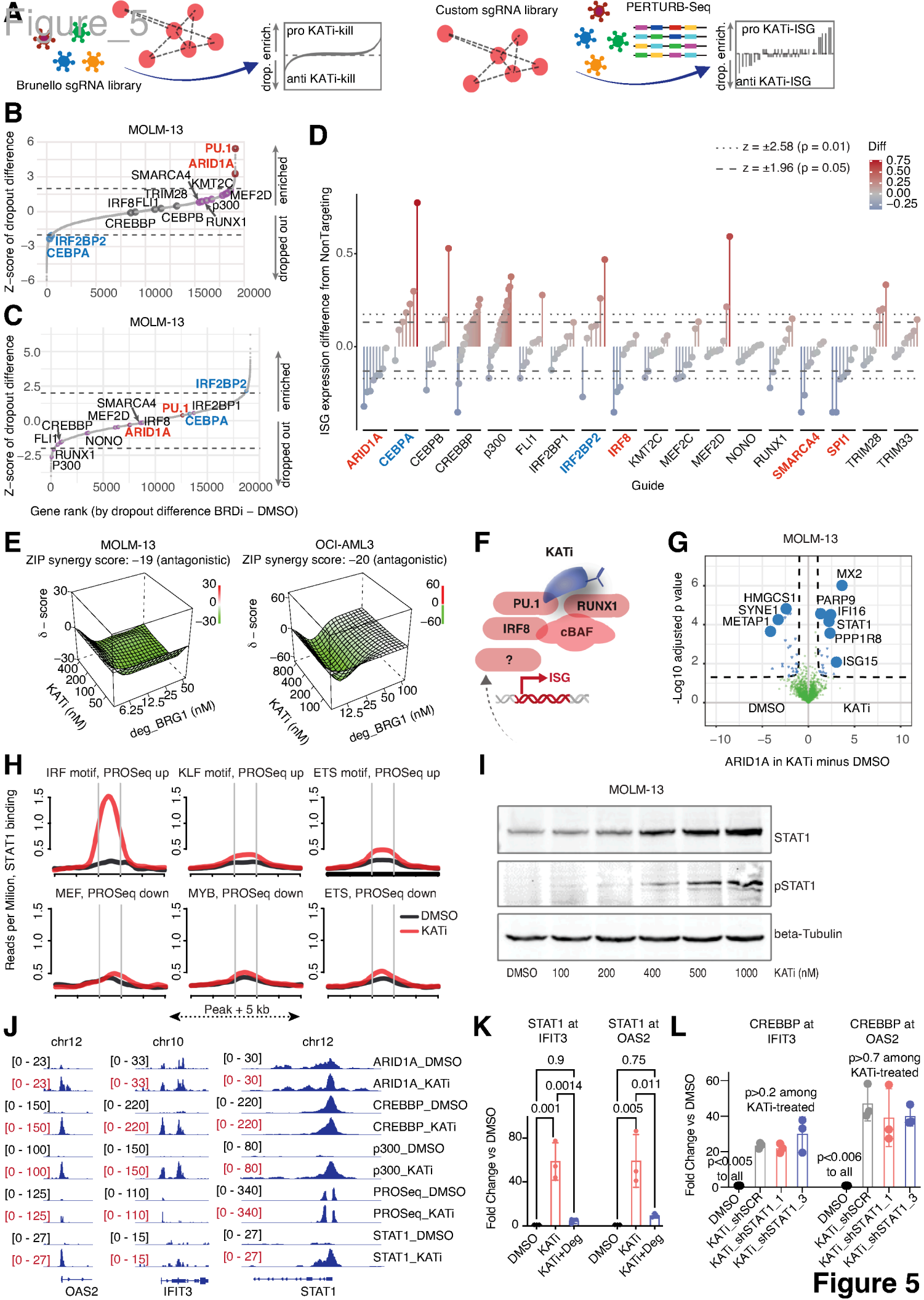
A
Brunello sgRNA library
drop. enrich.
pro KATi-kill
anti KATi-kill
Custom sgRNA library
PERTURB-Seq
pro KATi-ISG
anti KATi-ISG
B
MOLM-13
Z-score of dropout difference
PU.1
ARID1A
SMARCA4
KMT2C
TRIM28
MEF2D
IRF8
FLI1
p300
CREBBP
CEBPB
RUNX1
IRF2BP2
CEBPA
enriched
dropped out
C
MOLM-13
IRF2BP2
SMARCA4
PU.1
IRF2BP1
MEF2D
IRF8
CEBPA
CREBBP
ARID1A
FLI1
NONO
RUNX1
P300
Gene rank (by dropout difference BRDi – DMSO)
D
z = ±2.58 (p = 0.01)
z = ±1.96 (p = 0.05)
Diff
ISG expression difference from NonTargeting
Guide
ARID1A
CEBPA
CEBPB
CREBBP
p300
FLI1
IRF2BP1
IRF2BP2
IRF8
KMT2C
MEF2C
MEF2D
NONO
RUNX1
SMARCA4
SPI1
TRIM28
TRIM33
E
MOLM-13
ZIP synergy score: –19 (antagonistic)
OCI-AML3
ZIP synergy score: –20 (antagonistic)
δ – score
KATi (nM)
deg_BRG1 (nM)
F
KATi
PU.1
RUNX1
IRF8
cBAF
?
ISG
G
MOLM-13
-Log10 adjusted p value
MX2
HMGCS1
PARP9
SYNE1
IFI16
METAP1
STAT1
PPP1R8
ISG15
DMSO
KATi
ARID1A in KATi minus DMSO
H
IRF motif, PROSeq up
KLF motif, PROSeq up
ETS motif, PROSeq up
MEF, PROSeq down
MYB, PROSeq down
ETS, PROSeq down
Reads per Million, STAT1 binding
DMSO
KATi
Peak + 5 kb
I
MOLM-13
STAT1
pSTAT1
beta-Tubulin
DMSO
100
200
400
500
1000
KATi (nM)
J
chr12
chr10
chr12
ARID1A_DMSO
ARID1A_KATi
CREBBP_DMSO
CREBBP_KATi
p300_DMSO
p300_KATi
PROSeq_DMSO
PROSeq_KATi
STAT1_DMSO
STAT1_KATi
OAS2
IFIT3
STAT1
K
STAT1 at IFIT3
STAT1 at OAS2
Fold Change vs DMSO
0.9
0.0014
0.001
0.75
0.011
0.005
DMSO
KATi
KATi+Deg
L
CREBBP at IFIT3
CREBBP at OAS2
Fold Change vs DMSO
p>0.2 among KATi-treated
p<0.005 to all
p>0.7 among KATi-treated
p<0.006 to all
DMSO
KATi_shSCR
KATi_shSTAT1_1
KATi_shSTAT1_3

Figure 5

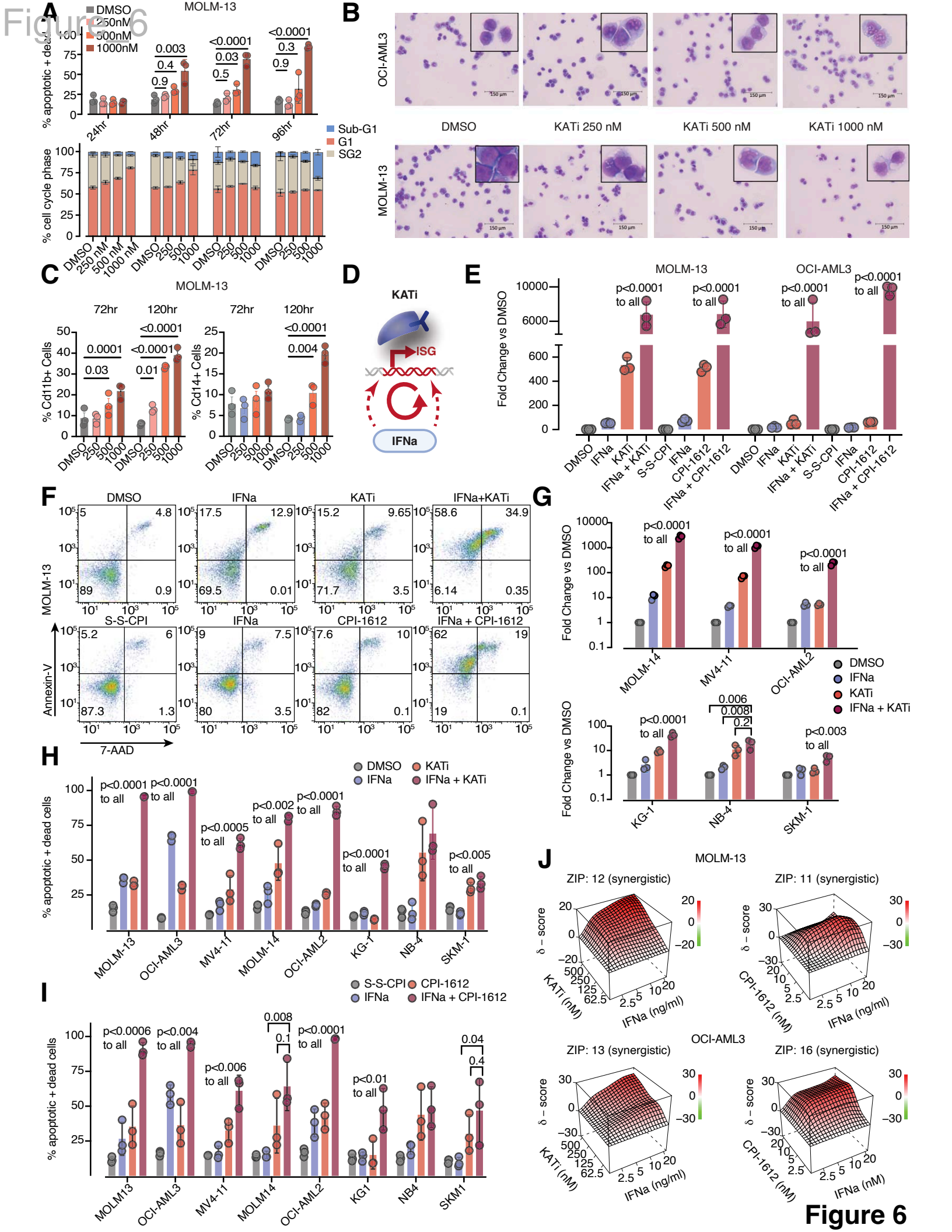
Figure 6
A
MOLM-13
DMSO
250nM
500nM
1000nM
% apoptotic + dead
0.003
0.4
0.9
<0.0001
0.03
0.5
<0.0001
0.3
0.9
24hr
48hr
72hr
96hr
Sub-G1
G1
SG2
% cell cycle phase
DMSO
250 nM
500 nM
1000 nM
B
OCI-AML3
MOLM-13
DMSO
KATi 250 nM
KATi 500 nM
KATi 1000 nM
C
MOLM-13
72hr
120hr
% Cd11b+ Cells
0.0001
0.03
<0.0001
0.01
% Cd14+ Cells
<0.0001
0.004
D
KATi
ISG
IFNa
E
MOLM-13
OCI-AML3
Fold Change vs DMSO
p<0.0001 to all
DMSO
IFNa
KATi
IFNa + KATi
S-S-CPI
CPI-1612
IFNa + CPI-1612
F
DMSO
IFNa
KATi
IFNa+KATi
S-S-CPI
CPI-1612
IFNa + CPI-1612
MOLM-13
Annexin-V
7-AAD
G
Fold Change vs DMSO
p<0.0001 to all
MOLM-14
MV4-11
OCI-AML2
DMSO
IFNa
KATi
IFNa + KATi
0.006
0.008
0.2
p<0.003 to all
KG-1
NB-4
SKM-1
H
% apoptotic + dead cells
p<0.0001 to all
p<0.0005 to all
p<0.002 to all
p<0.0001 to all
p<0.005 to all
MOLM-13
OCI-AML3
MV4-11
MOLM-14
OCI-AML2
KG-1
NB-4
SKM-1
I
S-S-CPI
CPI-1612
IFNa
IFNa + CPI-1612
% apoptotic + dead cells
p<0.0006 to all
p<0.004 to all
p<0.006 to all
0.008
0.1
p<0.0001 to all
p<0.01 to all
0.04
0.4
MOLM13
OCI-AML3
MV4-11
MOLM14
OCI-AML2
KG1
NB4
SKM1
J
MOLM-13
ZIP: 12 (synergistic)
ZIP: 11 (synergistic)
δ – score
KATi (nM)
IFNa (ng/ml)
CPI-1612 (nM)
OCI-AML3
ZIP: 13 (synergistic)
ZIP: 16 (synergistic)
IFNa (nM)
Figure 6

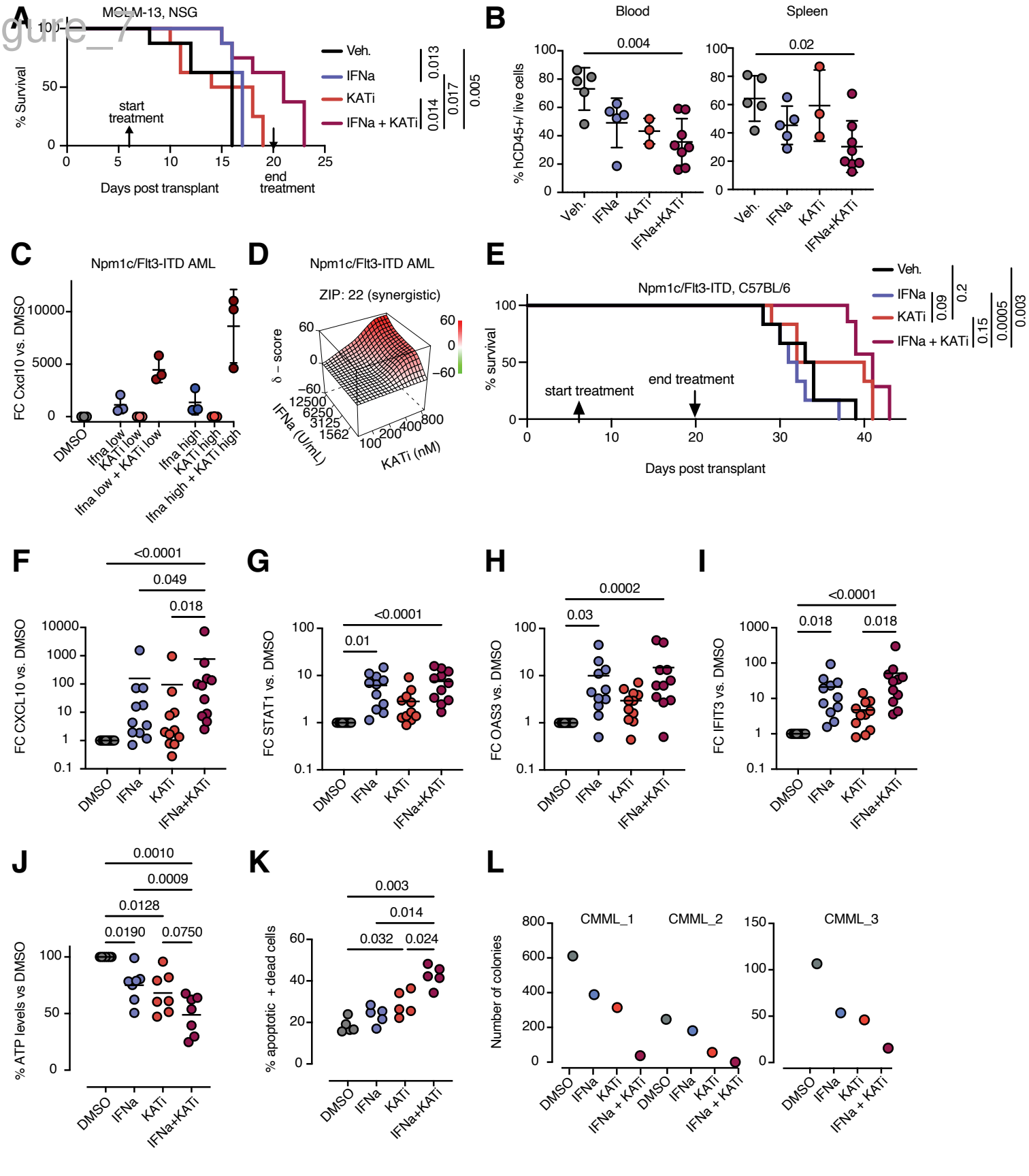
A
MOLM-13, NSG
% Survival
start treatment
end treatment
Days post transplant
Veh.
IFNa
KATi
IFNa + KATi
0.013
0.014
0.017
0.005
B
Blood
Spleen
% hCD45+/ live cells
0.004
0.02
Veh.
IFNa
KATi
IFNa+KATi
C
Npm1c/Flt3-ITD AML
FC Cxcl10 vs. DMSO
DMSO
Ifna low
KATi low
Ifna low + KATi low
Ifna high
KATi high
Ifna high + KATi high
D
Npm1c/Flt3-ITD AML
ZIP: 22 (synergistic)
δ – score
IFNa (U/mL)
KATi (nM)
E
Npm1c/Flt3-ITD, C57BL/6
% survival
start treatment
end treatment
Days post transplant
Veh.
IFNa
KATi
IFNa + KATi
0.09
0.2
0.15
0.0005
0.003
F
FC CXCL10 vs. DMSO
<0.0001
0.049
0.018
G
FC STAT1 vs. DMSO
<0.0001
0.01
H
FC OAS3 vs. DMSO
0.0002
0.03
I
FC IFIT3 vs. DMSO
<0.0001
0.018
0.018
J
% ATP levels vs DMSO
0.0010
0.0009
0.0128
0.0190
0.0750
K
% apoptotic + dead cells
0.003
0.014
0.032
0.024
L
Number of colonies
CMML_1
CMML_2
CMML_3

Figure 7